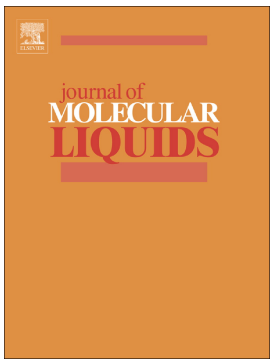

Solvent-free microwave assisted synthesis and corrosion inhibition study of a series of hydrazones derived from thiophene derivatives: Experimental, surface and theoretical study

A.K. Singh, S. Thakur, B. Pani, B. Chugh, H. Lgaz, Ill-Min Chung, P. Chaubey, A.K. Pandey, J. Singh

PII: S0167-7322(18)34856-6
DOI: https://doi.org/10.1016/j.molliq.2019.03.126
Reference: MOLLIQ 10667

To appear in: *Journal of Molecular Liquids*

Received date: 20 September 2018
Revised date: 30 December 2018
Accepted date: 22 March 2019

Please cite this article as: A.K. Singh, S. Thakur, B. Pani, et al., Solvent-free microwave assisted synthesis and corrosion inhibition study of a series of hydrazones derived from thiophene derivatives: Experimental, surface and theoretical study, Journal of Molecular Liquids, https://doi.org/10.1016/j.molliq.2019.03.126

Solvent-free microwave assisted synthesis and corrosion inhibition study of a series of hydrazones derived from thiophene derivatives: Experimental, Surface and Theoretical Study

A. K. Singh[1, *], S. Thakur[2], B. Pani[3], B. Chugh[2], H. Lgaz[4 *], Ill-Min Chung[4*], P. Chaubey[5], A. K. Pandey[2], J. Singh[1]

[1]Department of Applied Science, Bharati Vidyapeeth College of Engineering, New Delhi, India-110063
[2]Department of Chemistry, Netaji Subhash Institute of Technology, University of Delhi, New Delhi, India-110078
[3]Department of Chemistry, Bhaskaracharya College of Applied Science, University of Delhi, New Delhi, India-110078
[4]Department of Crop Science, College of Sanghur Life Science, Konkuk University, Seoul 05029, South Korea
[5]SVKM's Dr. Bhanuben Nanavati College of Pharmacy, Vile Parle (W), Mumbai, INDIA-400056

*Corresponding author
Tel. No. +919560285447
Email: ashish.singh.rs.apc@itbhu.ac.in

Abstract

A series of thiophene hydrazones namely acetyl thiophene benzohydrazide (ATBH), acetyl thiophene amino benzohydrazide (ATABH), propanoyl thiophene benzohydrazide (PTBH) and propanoyl thiophene amino benzohydrazide (PTABH) were synthesized by conventional as well as by energy efficient microwave irradiation exposure and investigated their potential to mitigate corrosion of mild steel in 0.5 M H_2SO_4 medium. The spectral and elemental analyses including FTIR, ^{1}H NMR, and CHN analysis were used to characterize synthesized hydrazones. The corrosion inhibition potential of the synthesized compounds was investigated by weight loss and several well known analytical tools such as open circuit potential (OCP), electrochemical impedance spectroscopy (EIS) and potentiodynamic polarization (PDP). Metal corrodes by charge

transfer mechanism across the interface of metal and acid solution and was found that addition of all the inhibitors to the acid solution reduced the corrosion rate appreciably. The inhibitor molecule showed a strong affinity for metal surface and adsorbed on its surface to offer resistance to flow of charge transfer across the interface of mild steel and acid solution. Langmuir adsorption isotherm was followed by adsorption of all the tested compounds. The thin films resulted due to adsorption of compounds on the metal surface were demonstrated by scanning electron microscope-energy dispersive X-ray (SEM-EDX), FTIR and X-ray photoelectron spectroscopy (XPS). Atomic force microscopy of mild steel surface was performed to examine the effect of inhibitors on its surface property. The contact angle measurement was also performed to examine the wettability of mild steel surface towards acid solutions. The experimental findings agreed well with the theoretical results performed by density functional theory (DFT). The interaction of inhibitors with mild steel, Fe (110) was investigated by MD simulations.

Key Words: Acid Corrosion, Energy Efficient Synthesis, X-ray photoelectron spectroscopy, SEM-EDX, EIS, Miller indices

1. Introduction

Generally, in nature, most of the metals are found in a chemically combined state known as ore. These ores represent their low energy state (thermodynamically stable state). The metals are extracted from these ores after applying a huge amount of energy. Metals in the uncombined condition (extracted form) have a higher energy and are in unstable state. They have their natural tendency to go back to the low energy state, i.e., combined state by recombining with the elements present in the environment which is the main reason of corrosion [1]. The worldwide significance of metals has attracted

attention of researchers to study about metallic corrosion. The impact of metallic corrosion append economic loss, damage of metallic equipment, contamination of products, accidents result in serious injury which may lead to loss of life.

Metals have become first choice to construct structures because of their mechanical strength which makes them strong enough to withstand in different environments. The problem of corrosion is not limited to iron only but almost all metals have a tendency to corrode because of their high energy thermodynamic state. In fact, there are a number of metals such as aluminum, zinc, chromium etc. corrode more readily compared to iron but they have a tendency of passivation [2]. These metals could have been the better choice to construct structures exposed directly to corrosive environment nevertheless mild steel has been used in a number of industries [3, 4] due to its optimum mechanical strength, malleability, weldability, and low cost.

Corrosion of metallic structures has always been a major issue because of huge economic loss associated with it. It also imposes a huge plight for public safety due to the collapse of buildings, bridges, etc. which result from corrosion. There are different possible ways to overcome or moderate the problem of corrosion like surface coating, inhibitors etc. The purpose of all the corrosion protection methods is to protect metals at the place of use. The use of organic compounds as corrosion inhibitor [5-8] is considered as simplest method due to its ease of use and cost-effectiveness. Thus, there is always a need to investigate novel substances that can retard the aggressiveness of corrosion in different environmental conditions/corrosive media.

Chemical synthesis has still been lively field as it could supply drugs and other materials to our society. Therefore, Chemical Scientists develop newer and newer

molecules with better properties to serve society in the best possible way. Throughout the history of the discovery of new entity, researchers have faced a series of obstacles. This could be too few chemical compounds to synthesize or it could be too many. Depending on the state of scientific knowledge at the time, these shortages and excesses of ideas and materials can result in bottlenecks in the discovery and development process of a new entity. Synthesis of new chemical entities is important in overcoming the bottlenecks in the discovery of new molecules. Chemical synthesis can bring about a number of changes such as minor modification of existing molecular framework to make new material or to modify existing route so that material can be synthesized more efficiently. The conventional methods of synthesis where the reactants were heated by a conventional source of heat energy have been very well documented and practiced so far. But these methods have some limitations as sometimes they result into a low yield of product and consume a huge amount of energy and time. Few new sources of heat energy were also introduced from time to time such as isomental, oil bath, water bath, and hot plate but the problems remain the same.

Recently, quite a few new methods viz. solid phase synthesis, microwave assisted and ultrasound assisted synthesis were employed and found very promising as far as economic and environmental problems are concerned. Microwave-assisted synthesis has been growing fast as a popular method in the research scientist community. Microwave directly transfers energy to the reactants [9] and not to the reaction vessel and due to its rapid heating, the formation of undesired products is prevented. Thus, microwave-assisted synthesis has been found a very fast and clean method of synthesis and provides efficient conversion of reactants to product [10, 11].

The corrosion inhibiting potential of a vast variety of organic compounds has been tested in different corrosive media. Schiff bases have always been a subject of intensive research as they show anti-malarial [12], antibacterial [13], antifungal [14], anti-cancerous [15] and corrosion inhibition property [16]. Schiff bases, especially those having thiophene nuclei as a part of their structure, can act as an initial unit to make a transistor, light emitting diodes and organic solar cells by synthesizing charge transporting molecules [17-19]. Thus, thiophene nucleus can be considered as a fast-growing potential unit in the world of heterocyclic chemistry having very promising characteristics. Due to the larger size of S-atom as compared to C, N and O atom, its lone pair of electrons can be delocalized more easily in the heterocyclic ring. Variety of biologically active complexes derived from Schiff bases with thiophene as their structural units have been extensively studied [20, 21].

Generally, tedious experimental procedures have to be performed to predict the corrosion inhibiting efficiency of organic compounds which may not be very cost effective as well as time-consuming. Therefore, we need alternatives on the basis of which we can predict their corrosion inhibition tendency without performing experiments. Density functional theory has been proved very promising to predict inhibition tendency of the molecule and to explore the inhibition mechanism.

In view of this, we have synthesized a series of thiophene hydrazones by the microwave-assisted method and investigated their performance against mild steel corrosion in the acid medium due to corrosion by different electrochemical as well as weight loss method. The experimental results were well compared and found consistent with the theoretical results.

2. Experimental

2.1 Synthesis of thiophene hydrazones

All the thiophene hydrazones were synthesized according to the previously discussed method [22]. The schematic representation of the synthesis of inhibitors and their structures are given as Fig. 1. The physical parameters and spectral characterization data are presented as Table 1.

An open capillary method was used to determine the melting points of all the synthesized compounds. The elemental composition was determined by CHN analysis performed by CHN analyzer. The CHN analyzer used was Exeter Analytical Inc. model CE-440. Jeol AL 300 FTNMR and JASCO FT/IR-5300 spectrophotometer were used to record the ^{1}H NMR and FTIR spectra of all the four synthesized compounds. The thin film of inhibitors formed due to their adsorption was also characterized by using JASCO FT/IR-5300 spectrophotometer.

2.2 Gravimetric analysis

Mild steel samples of $2.5 \times 2.0 \times 0.025$ cm^3were used to carry out gravimetric analysis. These samples were dipped for 3h in the electrolytic solution, i.e. 0.5 M H_2SO_4. The electrolytic solutions have different concentrations of inhibitors. After 3h, these samples were weighed to calculate the weight loss during an experiment. The gravimetric analyses were performed at four different temperatures i.e. 303 K, 313 K, 323 K, and 333 K to explain activation parameters as well as to throw the light about the effect of temperature on the process.

2.3 Electrochemical analyses

Gamry potentiostat/galvanostat (model 300) was used to run all the electrochemical measurements. The experimental set up consisted of three electrode cell- a saturated calomel reference electrode, Pt counter and mild steel working electrode [23]. The working temperature of all the experiments was kept constant at 303 K temperature. The mild steel strip, i. e. working electrode was dipped for 30 minutes in electrolytic solution before starting to run experiments. This 30 minute time was sufficient to stabilize the corrosion potential. The frequency range was fixed between 100000-0.01 Hz to run electrochemical impedance spectroscopy (EIS) under potentiostatic conditions. The EIS experiments were run at 10 mV peak to peak amplitude with AC signal at E_{corr}. The impedance spectroscopy data were analyzed by Echem analyst software. The potential range to run potentiodynamic polarization experiments was selected between ±250mV (SCE) and the scan rate was kept at 1 mV s^{-1}. The open corrosion potential was allowed was stabilized first and then all the electrochemical experiments were run.

2.4 Morphological study

2.4.1 Scanning electron microscopy-energy dispersive X-ray spectroscopy (SEM-EDX)

Scanning electron micrographs were scanned to get information about thin film deposited on the electrode surface due to adsorption of all the inhibitors which retarded corrosion of mild steel in an acidic electrolyte. Different electrolytic solutions were prepared by dissolving 400 mg L^{-1} concentration of all the inhibitors in 0.5 M H_2SO_4 separately. The working electrode samples were dipped in these solutions for 3h. Then these samples were taken out, dried and scanned by TM 3000 microscope to get SEM images and EDX. The TM 3000 microscope was fitted with EDX analyzer also. The acceleration voltage and working distance were selected at 5000 V and 8.5 mm,

respectively. The EDX spectra were recorded to analyze the film composition developed due to adsorption of inhibitors. The mild steel coupons taken out from inhibited solutions when dipped into 0.5 M H_2SO_4 showed protection from corrosion up to an appreciable extent which supports the view of film formation on the metal surface due to adsorption of inhibitors.

2.4.2 Atomic force microscopy (AFM)

AFM has emerged as an ever-important primary technique to study surface morphology. The surface morphology of electrodes immersed in the electrolytic solution and the effect of the addition of inhibitors to the solution has been widely studied by AFM in recent times [24]. The mild steel electrode samples were dipped in different electrolyte solution (0.5 M H_2SO_4 + 400 mg L^{-1} of inhibitor) separately for 3 h; taken out and then scanned topographical images in contact mode with atomic force microscope supplied from Bruker, USA.

2.4.3 FTIR spectroscopy

The thin film developed on the electrode surface due to adsorption of different inhibitors were removed first and then analyzed by recording FTIR spectra using JASCO FTIR-5300 spectrophotometer to confirm the thin film formation on the metal surface due to adsorption of inhibitors.

2.4.4 X-ray photoelectron spectroscopy (XPS)

The elemental composition of the film deposited on the surface and binding energy of the steel sample was confirmed by recording XPS spectrum of the mild steel specimen with ATBH. The XPS spectra were recorded by Omicron Multiprobe Surface

analysis System supplied from Germany. The pressure was kept 5×10^{-11}Torr to record XPS and the radiation source used was Mg Kα with an energy of 1253.6 eV.

2.5 Contact angle measurement

The hydrophilicity of the electrode surface to different electrolytic solutions was investigated by measuring its contact angle to the electrolyte. The contact angle measurement was done by Rame-Hart goniometer (Netcong) supplied from the US and the method used for measurement was static sessile drop method.

2.6 *Computational studies*

2.6.1 Quantum chemical calculation

DFT and MD simulations

The DMol^3 module associated with Materials Studio software (version 6.0) [25, 26] was used to perform all the quantum chemical calculations. In these calculations, the generalized gradient approximation (GGA) of the Perdew-Burke-Ernzerhof (PBE) formula was used for the electronic exchange-correlation potential [3], and all-electron calculations were performed with double-numeric basis set (DNP 4.4)[27]. The solvation effects (aqueous phase) was included in DMol^3 calculations by COSMO [28] controls. The ionization potential (IP) and the electronic affinity (EA) were derived from the energy associated with HOMO and LUMO [29]:

$$IP = -E_{\mathrm{HOMO}} \quad (1)$$

$$EA = -E_{\mathrm{LUMO}} \quad (2)$$

Using the values of IP and EA the electronegativity values and global hardness of inhibitor molecule can be calculated with the help of following equations [30]:

$$\chi = \frac{IP + EA}{2} \tag{3}$$

$$\eta = \frac{IP - EA}{2} \tag{4}$$

Using the Pearson method the number of transferred electrons (ΔN) can be calculated according to equation (5) [31]:

$$\Delta N = \frac{\phi - \chi_{\text{inh}}}{2(\eta_{Fe} + \eta_{\text{inh}})} \tag{5}$$

The values of ϕ obtained from DFT are 3.91, 4.82 and 3.88 eV for Fe (100), Fe (110) and Fe (111) surfaces, , respectively [32]. Here, we use only Fe (110) surface and the reason for this surface selection are its higher stabilization energy along with packed surface [33].

Further, the local reactivity of tested compounds has been further explored and detailed by computing Fukui functions [34]. With the help of finite difference approximations Fukui functions can be determined as [35]:

$$f_{\text{k}}^{+} = q_{\text{k}}(N+1) - q_{\text{k}}(N) \tag{6}$$

$$f_{\text{k}}^{-} = q_{\text{k}}(N) - q_{\text{k}}(N-1) \tag{7}$$

Here, q_{k} represents gross charge of *k* atom. The values of charge on anionic, cationic and neutral species are represented by $q_{\text{k}}(N+1)$, $q_{\text{k}}(N-1)$ and $q_{\text{k}}(N)$, respectively. In this study, Fukui functions have been expressed by using Mulliken population analysis (MPA).

A simulation box of dimension 24.82×24.82×35.69 $Å^3$ having 491H_2O, 9 SO_4^{2-} and 1 tested inhibitor molecule was used to perform MD simulations. All MD simulations

were performed using Materials Studio® software at temperatures T = 303K maintained constant by the Andersen thermostat, a time step of 1 fs, NVT ensemble and a simulation time of 2000 ps to reach simulation system under an equilibrium state. The energy minimization and MD calculations were achieved by using the COMPASS (Condensed-phase Optimized Molecular Potential for Atomistic Simulation Studies) force field [36]. The calculation of interaction and binding energy using equations 8 and 9 [37] enabled us to get information about the interactions between the tested inhibitors and Fe (110) surface:

$$E_{\text{interaction}} = E_{\text{total}} - (E_{\text{surface+solution}} + E_{\text{inhibitor}}) \quad (8)$$

$$E_{\text{binding}} = -E_{\text{interaction}} \quad (9)$$

Where, E_{total} represents the energy of the entire system, the $E_{\text{surface+solution}}$, denotes the entire energy of Fe (110) and the electrolytic solution in the absence of inhibitor molecules and $E_{\text{inhibitor}}$ denotes the whole energy of inhibitor molecules.

3. Results and Discussion

3.1 Synthesis

The synthesis of the inhibitors was achieved by carrying out reaction according to the scheme presented as Fig. 1. Initially, the products were synthesized by refluxing 0.015 moles of each A and B for 4-5 h in ethanol. Few drops of glacial acetic acid were added as a catalyst. The products were separated as a precipitate after cooling the reaction medium. The same reaction can be completed by exposure of microwave irradiation to a mixture of reactant A and B in presence of acid clay. After 3-5 minutes (min) exposure of microwave irradiation (MW) the product C separated in reasonably good yield (≈ 90%).

Thus, exposure to microwave irradiation provided very fast and clean route compared to conventional method of synthesis for the formation of these thiophene hydrazones.

3.2 Weight loss analysis

3.2.1 Relation of corrosion rate with inhibitor concentration

The 0.5 M H_2SO_4 solution showed very much aggressiveness against mild steel as seen by the corrosion rate (8.13 g cm^{-2} h^{-1}). The corrosion rate progressively slowed down when increasing amount of inhibitor added to 0.5 M H_2SO_4 solution as seen in Fig. 3. Thus, at high concentration of inhibitors, adsorption is more facilitated and thereby corrosion of metal is checked.

3.2.2. Temperature effect/ Activation parameters

To analyze the effect of altering temperature on the corrosion rate, weight loss experiments were performed at four different temperatures in the temperature range 303-333 K with temperature gap 10 K. The reaction kinetics of corrosion followed Arrhenius equation and transition state equation as follow [38]:

$$\log C_R = \frac{-E_a}{2.303RT} + \log \lambda \tag{10}$$

$$C_R = \frac{RT}{Nh} \exp\left(\frac{\Delta S^*}{R}\right) \exp\left(\frac{-\Delta H^*}{RT}\right) \tag{11}$$

Where, C_R is written for corrosion rate. All other terms such as E_a, λ, R, T, ΔS^*, ΔH^*, N and h have usual meaning of activation energy, Arrhenius factor, gas constant, absolute temperature, entropy of activation, enthalpy of activation, Avogadro's number and Planck's constant, respectively.

The activation energy and Arrhenius pre-exponential factor can be calculated from slope and intercept of the straight line obtained by plotting log C_R against $1/T$ as seen in Fig. 4a. The values of activation energy and Arrhenius factor obtained for 0.5 M H_2SO_4 solution and for all the inhibitors are listed in Table 2. The negative slope of this plot indicated adsorption of all the thiophene hydrazones and therefore the value of activation energy increased by the presence of these inhibitors and consequently the energy barrier to precede corrosion increased [39].

The values of the Arrhenius factor were also increased by the presence of compounds (as seen in Table 2) while they should be decreased for impeding corrosion. Thus, the decreased corrosion rate could be due to the dominant variation of activation energy [40].

The plot of log C_R/T *vs*. $1/T$ presented as Fig. 4b. The slope and intercept of the straight line obtained by plotting log C_R vs. $1/T$ provided the value of enthalpy and entropy of activation listed in Table 2. The value of enthalpy of activation, ΔH^*increased due to the presence of all the inhibitors which indicated that the minimum energy barrier to be crossed to take place corrosion is raised by the presence of all the inhibitors. Thus, the mild steel dissolution became difficult by the presence of these inhibitors.

The large negative value of entropy of activation (ΔS^*) indicated that this process passed through an intermediate state or transition state whose entropy is lowered by this value or in other words transition state represented association rather than dissociation [41]. The entropy of activation (ΔS^*) increased positively by the addition of all the inhibitors; maximum increment noticed for PTABH. The increased value of entropy of activation reduced the probability of attaining intermediate state or transition state [42] and hence the reduced corrosion rate.

3.2.3 Adsorption isotherm

The study about adsorption isotherm is one of the most important processes in corrosion inhibition using organic compounds because it is the adsorption isotherm which can enlighten about the mechanism of adsorption. Different adsorption isotherm models were tested to explain the experimental data. The equation which can explain the entire isotherm in general as [41]:

$$f(\theta, x)\exp^{(2a\theta)} = K_{ads}C_{inh} \quad (12)$$

where, K_{ads} is adsorption constant, C_{inh} is inhibitor concentration, θ is the fraction of metal surface covered with inhibitor molecule and $f(\theta, x)$ is a physical model dependent configurational factor.

Langmuir adsorption isotherm explained the experimental results in a perfect way as its slope and linear regression coefficient was found close to unity. Langmuir adsorption isotherm is one of the simplest models which assume homogeneous and independent single layer adsorption as well as ideal solutions. This isotherm is based on assumption that no interaction involved inhibitor molecules adsorbed on the electrode surface. This isotherm can be presented by an equation as [43]:

$$\frac{C_{inh}}{\theta} = \frac{1}{K_{ads}} + C_{inh} \quad (13)$$

The description of experimental data with Langmuir isotherm is presented in Fig. 4c. The intercept of this plot provided the value of K_{ads} which measures the adsorbing capacity of inhibitor or strength of its adsorption. By means of adsorption equilibrium constant, K_{ads}, the calculation of free energy of adsorption (ΔG^{o}_{ads}) can be done with the help of equation (14) as [44]:

$$\Delta G^{o}_{ads} = -RT \ln(55.5 K_{ads}) \quad (14)$$

Where, ΔG^{o}_{ads} is free energy of adsorption which gives an idea about the spontaneity of the adsorption process, *T* stands for absolute temperature, 55.5 represents molar strength of water in solution and R is gas constant.

The values of adsorption parameters are presented in Table 3. A number of previous studies [45, 46] reported that the value of standard free energy of adsorption gives an idea about the spontaneity of the process as well as nature of interaction among the inhibitor molecules adsorbed at the electrode surface. The value of ΔG^{o}_{ads} <20 kJ mol^{-1} usually associated with pure electrostatic interaction i.e. physical adsorption while values >40 kJ $mol^{-1}$to chemical interaction through charge transfer or charge sharing [47]. In present study, the value of standard free energy of adsorption obtained (at 303 K) for ATBH, PTBH, ATABH and PTABH were found to be 28.4, 28.9, 29.2 and 29.8; , respectively which indicate that these inhibitors were adsorbed on the electrode surface not only through electrostatic interaction or chemical interaction but they were adsorbed through the mixing of both types of interactions. The increasing values of standard free energy of adsorption for ATBH, PTBH, ATABH, and PTABH indicate their increasing adsorption capacity and thus their order of efficiency. These molecules can exist in two forms: as a neutral molecule and as a protonated molecule. The neutral molecule is adsorbed chemically by transfer or sharing of electrons while charged protonated molecules are adsorbed electrostatically by the interaction between oppositely charged metal surface and the inhibitor molecules.

Further adsorption thermodynamic parameters such as enthalpy and entropy for adsorption process were calculated to enlighten about adsorption of the inhibitor

molecules. The gravimetric experiments were performed in the temperature range of 303-333 K separated by 10 K with 400 mgL^{-1} concentration of all the tested inhibitors to calculate the thermodynamic adsorption parameters. Van't Hoff equation can be used to calculate these parameters as [48]:

$$\ln K_{ads} = \frac{1}{55.5} + \frac{-\Delta H^0_{ads}}{RT} + \frac{\Delta S^0_{ads}}{R} \qquad (14)$$

Where, all the symbols K_{ads}, ΔH^0_{ads}, ΔS^0_{ads}, R and T have their usual meaning.

The plot of ln K_{ads} *vs.* 1/T provided a straight line and presented as Fig. 4d. The slope (= $-\frac{\Delta H^0_{ads}}{R}$) and intercept of this line enabled to calculate enthalpy and entropy of adsorption. The calculated values of ΔH^0_{ads} and ΔS^0_{ads} for all the inhibitors, ATBH, PTBH, ATABH, and PTABH are given in Table 3. The exothermic nature of adsorption of inhibitors was confirmed by the negative value of enthalpy of adsorption while the positive value of entropy of adsorption indicated that the adsorptions of inhibitors were mainly controlled by the entropy of adsorption. The positive entropy reflected the strong interaction of adsorbate i.e. inhibitors with the adsorbent surface, i.e. mild steel. The increment of entropy is attributed to solvent entropy [49], i.e. increased randomness of water molecules. The adsorption of tested inhibitors is a quasi-substitution process includes the adsorption of inhibitors present in the electrolytic solution to the electrode surface at the cost of desorption of already adsorbed solvent molecules, i.e. water molecules. Thus, the complete process includes a decrease in entropy of inhibitors and the increase in entropy of solvent. The resultant entropy is the sum of the entropy of

inhibitor and solvent and therefore positive entropy is the result of solvent entropy increment.

3.3 Electrochemical parameters

3.3.1 Electrochemical impedance spectroscopy (EIS)

Impedance spectroscopy (EIS) has been very informative to deduce the information regarding the mechanism of corrosion inhibition. The performance of inhibitor on the basis of EIS can be given by equation as:

$$P_{\mathrm{EIS}}\% = \frac{R_{\mathrm{ct}}^{\mathrm{i}} - R_{\mathrm{ct}}^{0}}{R_{\mathrm{ct}}^{\mathrm{i}}} \times 100 \qquad (15)$$

Where, the symbol $R_{\mathrm{ct}}^{\mathrm{i}}$ and R_{ct}^{0} denote charge transfer resistance with organic compound tested as a corrosion inhibitor and charge transfer resistance in mere H_2SO_4 acid solution, respectively.

The impedance behavior of mild steel in the experimental solution with the different amount of all the four organic compounds namely ATBH, PTBH, ATABH, and PTABH were tested and the results presented as Table 4. The EIS spectra of mild steel (MS) in tested acid solution with 400 mg L^{-1} (all other results data are given in the Table 4.) of tested compounds are presented as Fig. 5a-c. The Nyquist plots contain a single semicircle only whose diameters reflect the value of R_{ct}. The increasing diameter of Nyquist plots by addition of increasing amount of each inhibitor separately indicated that their corrosion mitigating potential increases with their amount in the acid solution [50, 51]. The order of ability to mitigate corrosion was found as ATBH < PTBH < ATABH < PTABH. Fig. 5a shows Nyquist plots of MS with optimum concentration i.e. 400 mg L^{-1} together with that in 0.5 M H_2SO_4 solution. The shape of these capacitive loops is not real

semicircle instead of a depressed one. This depression is the characteristic effect of surface roughness or inhomogeneity of MS electrode and is only due to the frequency dispersion effect of the electrode [52]. The performance of double layer capacitance is not like ideal capacitance. Thus, the appropriate circuit, which is required to analyze the impedance, results by fitting the experimentally obtained graphs involve constant phase element (CPE) instead of C_{dl} together with surface inhomogeneity regulatory factor (n). The equivalent circuit which is used to fit the experimental results in this study presented as Fig. 4d. The EIS parameters obtained after fitting all the experimental data with the proposed circuit is presented in Table 4.

The total impedance of *CPE* is calculated using equation (16) as [53]:

$$Z_{\mathrm{CPE}} = Y_0^{-1}(j\omega)^{-\mathrm{n}} \qquad (16)$$

Where, Y_0 represents CPE extent, n having a value of $0 < n < 1$ is the phase shift, j represents an imaginary number while ω is the angular frequency with a maximum value of Z_i. The electrochemical behavior of any system is principally decided by the value of n. If $n = 1$, the system behaves like an ideal capacitor, i.e. $Y_0 = C$; if $n = 1/2$, CPE behaves like a Warburg impedance, i.e. $Y_0 = \sigma$; $Y_0 = 1/R$ when $n = 0$; and $1/Y_0 = L$ if $n = -1$.

The Bode-phase plots of MS in acid solution presented as Fig. 4b &c. The Bode plots showed that the lower frequency impedance modulation was increased by the addition of all the four compounds. The maximum increment was noted for PTABH. As shown in Fig. 4c, the maxima of phase angle plot is increasing regularly by the presence of inhibitors namely ATBH, PTBH, ATABH, and PTABH. The increasing phase angle in the presence of these inhibitors confirmed their capacitive behavior. The order of the

increment is as follow: 0.5 M H_2SO_4< ATBH < PTBH < ATABH < PTABH. This is also their effectiveness order against corrosion in 0.5 M H_2SO_4 electrolyte solution.

3.3.2 Polarization behavior study

Potentiostatic method has been basically succeeded by potentiodynamic polarization study due to its time-consuming nature. Tafel polarization is generally carried out to get some information about the mechanism of electrode reactions, the role of inhibitors, activation energy, and other energy aspects. The superiority of the polarization method over other methods is closely related to the fact that it enables us to measure instantaneous reaction rates at metal-solution interface from a single experiment.

The polarization curves of mild steel obtained after running the experiments in 0.5 M H_2SO_4 solution with 400 mg L^{-1} of all the four inhibitors, i.e. ATBH, PTBH, ATABH and PTABH along with that in acid solution only are presented as Fig. 6. The data obtained by extrapolating cathodic and anodic polarization curves at all the concentrations of tested inhibitors are listed in Table 5.

The equation used to compare the corrosion inhibiting potential of tested inhibitors as [54]:

$$P_{\mathrm{PDP}}\% = \frac{i^{0}_{\mathrm{corr}} - i^{\mathrm{i}}_{\mathrm{corr}}}{i^{0}_{\mathrm{corr}}} \times 100 \qquad (17)$$

Where, i^{0}_{corr} and $i^{\mathrm{i}}_{\mathrm{corr}}$ stands for the value of corrosion potential for the bare acid solution and inhibited acid solution, respectively.

Fig.6 confirmed the reduction of corrosion current density by the presence of all the tested inhibitors, i.e. ATBH, PTBH, ATABH, and PTABH. The corrosion current density continued to reduce with the gradually increasing amount of inhibitors as seen in

Table 5. The occurrence of almost parallel cathodic polarization curves indicates that the mechanism of cathodic reactions has not changed significantly. Thus, these inhibitors lessened the corrosion rate by covering the active sites (responsible for corrosion) present on the electrode surface. Also, insignificant change (< 85 mV) of corrosion potential (E_{corr}) occurred by the addition of inhibitors compared with that of blank acid solution; it indicated that these tested inhibitors classified as mixed type inhibitors. Similar findings have also been reported for other organic inhibitors by other authors [55, 56]. These inhibitors control both anodic as well as cathodic reactions of corrosion as indicated by an alteration of anodic and cathodic Tafel slopes. The difference in anodic Tafel slope might be due to a change of chemical to the electrochemical mechanism. However, the shifting of corrosion potential in the cathodic region confirmed predominant cathodic nature of tested inhibitors. The results obtained from different methods are consistently similar to each other as presented in Table 6.

3.4 Morphological study approach

3.4.1 Scanning electron microscopy

The high definition SEM images of the surface of different mild steel samples which were immersed in acid solution only and with 400 mg L^{-1} concentration of all the compounds, ATBH, PTBH, ATABH, and PTABH were obtained from FE-SEM are displayed as Fig. 7. The mild steel immersed in acid solution only got damaged and scratched terribly while those immersed in the solution with inhibitor remained smooth and protected appreciably by the use of all these inhibitors. However, the protection is more noticeable with ATABH and PTABH as shown in Fig. 7d & e. This is according to their corrosion inhibiting potential; as ATABH and PTABH both showed excellent action

against acid corrosion. The order of efficiency of the compounds is as ATBH< PTBH< ATABH< PTABH.

3.4.2 Energy-dispersive X-ray spectroscopy

Energy-dispersive X-ray spectroscopic analysis was done to ascertain the presence of the elements on the electrode surface after immersing in acid solutions with and without inhibitors. The EDX spectrum of mild steel immersed in acid solution only shows characteristic peaks of its constituent elements (Fig. 7a*) while those of mild steel samples immersed in inhibitor solution (Fig. 7 b*-e*) shows peaks of C, O, N and S also, which indicates that the inhibitors molecules involved in bonding with mild steel electrode surface through these atoms. This fact is further supported by the findings of the IR and XPS spectra of the film removed from the electrode surface (discussed later in section 3.4.4 and 3.4.5 respectively).

3.4.3 Atomic force microscopic analysis

Atomic force microscopy was used to analyze surface features for the first time in 1986. The advantage of using AFM for the surface study is to facilitate the analysis at the micro- to nanoscale and even at the molecular level. AFM has emerged as an important topography analyzing tool as it allows the measurement of surface roughness. The three dimensional (3D) topographical images of electrodes recorded by AFM are presented as Fig. 8a-e. The surface of mild steel exposed directly to the acid solution (Fig. 8a) got damaged terribly as it shows rougher and porous surface (average surface roughness = 568 nm) compared to others which were immersed in inhibitor solutions. The surface of mild steel electrodes dipped in different inhibitor solutions remained smooth and thus showed protection from corrosion by the application of these inhibitors. The surface

roughness of the electrode surface immersed in different inhibitor solutions was found to be 326, 268, 228 and 181 nm for ATBH, PTBH, ATABH, and PTABH, respectively as shown in Fig. 8b-e. The values of surface roughness were according to the corrosion inhibiting potential of these inhibitors, i.e. ATBH < PTBH < ATABH < PTABH.

3.4.4 FTIR spectroscopy

To understand the interaction of mild steel surface with inhibitors, IR spectra of inhibitor film removed from the surface were run. The IR spectra of original inhibitor and removed inhibitors film are presented as Fig. 2a & b, respectively. The prominent peaks obtained in the recorded spectra of the original compounds ATBH, PTBH, ATABH and PTABH due to the presence of various characteristic functional groups appeared in the spectra of films removed from the electrode surface. However, these peaks shifted marginally as compared to the IR spectra of original compounds. The presence and shifting of these peaks in the spectra of films removed from the metal surface ensured the interaction of inhibitors with the mild steel surface leading to the complex formation which resulted into metal protection against aggressive corrosion.

3.4.5 X-ray photoelectron spectroscopic study

To confirm the nature of organic film developed due to adsorption of inhibitors, XPS analysis was done with the mild steel sample dipped in ATBH solution. The XPS spectra of mild steel immersed in 0.5 M H_2SO_4 solution with an optimum concentration of ATBH is shown in Fig. 9 a-e. The XPS spectra of the film deposited on the electrode surface (Fig. 9a) contains multiple peaks for different elements like S 2p, C 1s, N 1s, O 1s and Fe $2p_{3/2}$ which confirms the adsorption of inhibitor ATBH on the electrode

surface. The high-resolution spectra for different elements like S, C, N, O, and Fe are presented as Fig. 9b, c, d, e & f, respectively.

The XPS spectrum of S consists of two peaks as shown in Fig. 9b. These two peaks were observed at 168.5 and 169.75. The first peak at 168.5 is probably attributed to S-Fe complex while the second peak at 169.75 assigned to adsorbed metal sulfate.

The deconvoluted C 1s spectra of acid immersed mild steel having ATBH inhibitor (Fig. 9 c) shows three peaks; the first peak at 284.74 is assigned to C-C, C=C and C-H part of aromatic ring, the second obtained at 286.26 is attributed to C=N and C-S of thiophene ring and the third peak (288.22) obtained at slightly higher energy is either attributed to carbon atom of $C=N^+$ and C=O. This contribution of $C=N^+$ for this peak is resulted either from protonation of C=N bond and/or due to coordination of N_9 with the mild steel surface.

The Fig. 9d presented N 1s spectrum consist of two peaks: first at 399.4 assigned to C-N and =N- part of ATBH, i.e. unprotonated nitrogen atom. The second peak observed at 400.5 attributed to coordination of N-atom with Fe to form a complex. This coordination might have taken place between =N- part of ATBH and/or –N- part with Fe.

The O 1s spectrum of electrode surface immersed in acid-ATBH solution consists of two peaks (Fig. 9e): the first one at 529.7 is attributed to O^{2-}which is involved in the metal oxide formation (Fe_2O_3 or Fe_3O_4) while the second one at 531.8 is assigned to FeOOH or oxygen of adsorbed water molecules.

The Fe $2P_{3/2}$ spectrum exhibits three peaks at 711.52, and 715.63. The peak at 710.8 assigned to Fe^{3+} i.e. Fe^{3+} oxides or hydrous iron oxides while the peak observed at 715.63 assigned to the satellite of Fe (III).

Thus, the XPS analysis of mild steel immersed in inhibitor ATBH solution confirms its adsorption on the electrode surface. Further, the formation of an insoluble and stable layer of Fe^{3+} products, i.e. Fe_2O_3 and FeOOH retarded the diffusion of ions across the layer which resulted into reduced corrosion rate.

3.4.6 Study of wetting behavior of surface

To understand the wetting behavior of the electrode surface with different inhibitor solution, contact angles of the metal surface to the all the solutions were measured. The result obtained is presented as Fig. 10. The contact angle progressively increases by the presence of increasing amount of inhibitors in the solution and hence confirms decreased affinity of the metal surface to the inhibitor solution as compared to the acid solution only. The order of contact angle obtained for different inhibitors solution is ATBH < PTBH < ATABH < PTABH which is the same as that of their corrosion inhibiting potential.

3.4.7 Quantum chemical calculation

3.4.7.1DFT calculations

3.4.7.1.1Global reactivity descriptors

Quantum chemical calculations (QCC) have been proposed as a promising tool to explain and interpret observations in different experiments. In corrosion research, the QCC was successfully used to explain and predict a large number of known molecular parameters directly associated with the inhibitive performance of corrosion inhibitors [57]. In this investigation, theoretical calculations were used to get fundamental insights into the effect of functional groups on the effectiveness of tested inhibitors. Theoretical calculations were done using DFT in the liquid phase and the results are depicted in Fig.

11 and Table 6. Highest occupied molecular orbital (HOMO) and Lowest unoccupied molecular orbital (LUMO) (Fig.11) play an important role in determining the most reactive regions in the inhibitor molecule. HOMO is referred to as the orbital that could act as an electron donor while LUMO is the orbital that could act as the electron acceptor [58]. Here, it could be readily observed that the electron density distribution in the HOMO of ATBH, PTBH, and PTABH is mostly concentrated on the thiophene moiety and nitrogen atoms, though we observe some electron density distribution from other atoms. Interestingly, the electron density distribution in the HOMO of ATABH has moved towards aniline moiety. Compared to HOMO, the electron density distribution in the LUMO of all inhibitors is localized almost on the entire molecular structure except in inhibitor ATABH that is mainly concentrated on thiophene and N atoms. These electron density distributions of the HOMO and LUMO surfaces suggest that possible interactions have occurred mainly when the inhibitor molecules are in close contact with the steel surface. Further, these results revealed the interactions between inhibitor molecules and metal surface have occurred via donation and back-donation of the electrons as well as by electrostatic interactions.

There have been a number of successful explanations regarding the metal-inhibitor interactions from the molecular orbital theory viewpoint. Important properties of inhibitor molecules can be clarified by elucidating the mechanism of metal-inhibitor interactions on the basis of the HOMO and LUMO energy as well as energy gap [59]. E_{HOMO} is a significant molecular characteristic that determines the nucleophilic ability of the inhibitor molecule. There is now a general consensus that E_{HOMO} could conclude the possibility of a reaction by an electrophilic attack. In other words, a higher value of

E_{HOMO} would facilitate the electron-donating ability, so that the heteroatoms from inhibitor molecule would easily transfer their electron to a metal surface [60]. E_{LUMO} indicates a higher tendency of the inhibitor molecule to receive electrons from the metal surface [59]. On the other hand, the LUMO orbitals could form π-back bonds by accepting electrons from the metal using $\pi*$ orbitals. It can be inferred from Table 6 that the inhibitor PTABH has the highest value of $E_{HOMO,}$ indicating the highest tendency of donating electrons to the iron atoms. This strongly demonstrates that the assembly of both amino and ethyl groups is primarily the reason for the enhanced donating ability and therefore, increased inhibition performance. On the other hand, inhibitor ATABH has certain differences compared to inhibitor PTABH which means that amino group acts more effectively than an ethyl group, while inhibitor ATBH has the lowest donating ability. The results listed in Table 7 suggest that E_{LUMO} values do not show any trend towards an increase or decrease in electron accepting ability with the inhibition efficiency. The electron donating ability of inhibitors play the crucial role in the adsorption extent, thus in the inhibition performances of tested compounds. However, it remains clear that HOMO distribution provides insight knowledge to the role of the tendency of electron accepting of each inhibitor and indicates that the inhibitors prefer to form π-back bonds also and are not only an electron-donating agent. The energy difference between the HOMO and the LUMO energies is known as a HOMO-LUMO gap (ΔE). ΔE is one of the key factors determining the reactivity of the inhibitor molecule. The smaller the value of ΔE, the greater the reactivity of an inhibitor molecule [61]. The values of ΔE of all inhibitor molecules are close to each other, but PTABH has a lower ΔE value, confirming its greater ability to inhibit the corrosion of iron.

Additionally, it is noted that an inhibitor molecule transfers its electrons to metal if $\Delta N > 0$ and vice versa if $\Delta N < 0$ [62]. Therefore, according to this criterion, the results in Table 7 shows that all inhibitor molecules have the tendency to donate electrons to the metal surface. Further inspection of the results revealed that the ΔN values follow the same trend of the HOMO energy, indicating that all compounds exert their action preferably by donating electrons to the metal surface.

Overall, it is clear that small changes in the substituents of the inhibitor molecule led to an interesting reactivity profile. The experimental results show that the inhibition efficiency for studying compounds follows the order; PTABH > ATABH > PTBH > ATBH which implies that compound PTABH has the highest corrosion inhibition tendency. In addition to the common reactive sites, the highest reactivity of the compound PTABH is due to the presence of amino and ethyl groups on its molecular structure and thus enhancing its interactive strength. In the case of compound ATABH, the presence of amino group on its molecular structure makes it more reactive than compounds PTBH and ATBH. It is well-known fact that functional groups containing heteroatoms considerably increase the interactive ability of a corrosion inhibitor.

3.4.7.1.2 2.2 Fukui functions

Local reactivity analysis could gather more detailed information about the most reactive sites in each inhibitor molecule. The Fukui functions were calculated on the basis of Mulliken population analysis [63]. In this concept, Fukui function expresses the sensitivity of the atomic site of a chemical compound towards donation and acceptation of an electron and this can be correctly evaluated by the electrophilic and nucleophilic Fukui function values, respectively. Higher the value of Fukui function at a particular

site, higher is its local reactivity [63]. The results are summarized in Table 8 from which we notice that in all inhibitor molecules, the sulfur atom possesses high values of f_k^+ and f_k^- (except in PTBH), indicating that the thiophene moiety has generally greater contribution in accepting and donating of electrons, while the aniline moiety is mainly responsible on the electron donating ability of inhibitor PTBH. Other reactive centers are distributed over the entire molecular structure of inhibitors. The results obtained for these regions in nucleophilic and electrophilic attacks are in good agreement with the distribution of HOMO and LUMO orbitals and support the high capability of tested compounds to react with the surface of metal through donor-acceptor interactions between their reactive sites and steel surface.

3.4.7.1.3 *Molecular Dynamic (MD) simulations*

During the recent years, molecular dynamics simulations have proven to be a versatile technique for the simulation of a large number of corrosion inhibition systems enabling the correlation of the extent of adsorption with experimentally-observed corrosion inhibition [64]. Of course, this leads to a deep molecular understanding of the interactions between the inhibitor molecules and the metal surface. In the followings, we perform the molecular dynamics calculation on the adsorption of the inhibitors on the steel surface. In order to mimic the experiment, the corrosive particles along with water molecules are implemented in the simulation system. The system reaches equilibrium only if both energy and temperature reach balance [65]. Fig. 12 shows the most stable low energy adsorption configurations of the inhibitors on Fe (110). From the results, one can see a close contact between all inhibitors and the iron surface which is indicative of a strong interaction between them. It is common knowledge that heteroatoms-containing

functional groups pretentiously affect the adsorption ability of corrosion inhibitors, thus their inhibitive performances. In our present case, indeed, this effect was clearly observed. The strongest effect was exerted by the thiophene and aniline moieties as well as nitrogen atoms.

The interaction energies and the binding energies of interaction in systems are listed in Table 9. An interesting point in this data is that the values of the interaction energy of all inhibitor molecules are close to each other which can be explained in two ways: by a small difference in the molecular structure of compounds, and/or by the presence of the thiophene moiety in all compounds, which can ensure a strong binding with iron atoms as observed in Fukui functions results. A high value of interaction energy for inhibitor PTABH reflects the higher stability of its adsorption [59]. Further, we note that all inhibition systems are associated with strong, stable and spontaneous adsorption on Fe(110) surface [66]. Also, the high magnitude of the binding energy indicates that the inhibitor molecules adsorbed through more than one adsorption centers [67, 68]. Here again, it is worth noting that the highest correlation was observed with experimental and DFT results.

4. *Conclusions*

Thiophene derived hydrazones have been synthesized conventionally as well as by microwave-assisted method. Their corrosion inhibiting potential has also been investigated. This study resulted into following conclusions:

1. The microwave-assisted method of synthesis is found superior compared to conventional one as it leads to a high yield of the products and also consumes much less time.

2. All the thiophene derived hydrazones were found to have excellent potential to mitigate corrosion of mild steel in different acid media. The inhibiting potential of these compounds was the function of their amount added to the corroding medium.
3. The insignificant shift of corrosion potential as revealed by Tafel polarization confirmed the mixed type nature of these inhibitors. The increasing values of R_{ct} by the addition of increasing amount of inhibitors showed that they adsorbed effectively on the electrode surface.
4. Langmuir isotherm has been followed by the adsorption of all these inhibitors ATBH, PTBH, ATABH, and PTABH. The high value of adsorption constant confirmed the strength of their adsorption.
5. The formation of the film due to adsorption of these compounds was assessed by AFM, SEM-EDX, FTIR and XPS spectra of investigated mild steel surface.
6. The experimental findings were well corroborated by theoretical density functional theory (DFT) and molecular dynamics (MD) studies.

Acknowledgment

Author AKS is grateful to Bharati Vidyapeeth's College of Engineering to provide a platform to carry out research work. We are also thankful to our colleagues from respective Institution who assisted directly or indirectly for this research work. The authors are immensely grateful to reviewers for their comments that greatly improved the manuscript.

Conflict of interest

No conflict of interest to declare.

Caption of Figures

Fig. 1 Schematic representation of the synthesis of all the inhibitors and their chemical structures

Fig. 2 (a) IR spectra of all the four compounds, (b) IR spectra of the film removed from the surface of electrode dipped in the solution of different inhibitors and (c) ^{1}H NMR spectra of all the four inhibitors

Fig. 3 Variation of corrosion rate against the concentration of different inhibitors

Fig. 4 (a) Plot of log C_R vs. 1/T, (b) Plot of log C_R/T vs. 1/T (c) Langmuir adsorption isotherm for the adsorption of different inhibitors on the mild steel surface and (d) adsorption isotherm plot for ln K_{ads}*vs.* 1/T

Fig. 5 (a) Effect of the presence of 400 mg $L^{-1}$of all the inhibitors in 0.5 M H_2SO_4 solution on Nyquist plots, (b) Effect of the presence of 400 mg $L^{-1}$of all the inhibitors in 0.5 M H_2SO_4 solution on Bode plots, (c) Effect of the presence of 400 mg $L^{-1}$of all the inhibitors in 0.5 M H_2SO_4 solution on Nyquist plots and (d) Equivalent circuit used to analyze the experimental data

Fig. 6 Effect of the presence of inhibitors on potentiodynamic polarization curves of mild steel in 0.5 M H_2SO_4

Fig. 7 Scanning electron micrograph and EDX spectrum of mild steel immersed in (a &a*) 0.5 M H_2SO_4, (b & b*) 0.5 M H_2SO_4 + 400 mg L^{-1} of ATBH, (c & c*) 0.5 M H_2SO_4 + 400 mg L^{-1} of PTBH, (d & d*) 0.5 M H_2SO_4 + 400 mg L^{-1} of ATABH and (e & e*) 0.5 M H_2SO_4 + 400 mg L^{-1} of PTABH

Fig. 8 Atomic force micrograph of mild steel immersed in (a) 0.5 M H_2SO_4, (b) 0.5 M H_2SO_4 + 400 mg L^{-1} of ATBH, (c) 0.5 M H_2SO_4 + 400 mg L^{-1} of PTBH, (d) 0.5 M H_2SO_4 + 400 mg L^{-1} of ATABH and (e) 0.5 M H_2SO_4 + 400 mg L^{-1} of PTABH

Fig. 9 XPS spectra of mild steel surface removed after immersion in 0.5 M H_2SO_4 with 400 mg L^{-1} of ATBH: (a) survey scan spectra, (b) narrow scan spectra of S, (c) C, (d) N, (e) O and (f) Fe

Fig. 10 Variation of the contact angle of the electrode surface with the concentration of different electrolytic solutions

Fig. 11 Optimized structures, HOMOs, and LUMOs of ATBH, ATABH, PTBH, and PTABH

Fig. 12 Side views and top views of the model structures simulating the adsorption of ATBH, ATABH, PTBH and PTABH on the Fe (110) surface

References

[1] R. B.Mears, R. H.Brown, Ind. Eng. Chem.1941, 33, 1001-1010

[2] H. E.Townsend, R. G.Hart, J. Electrochem. Soc. 1984, 131, 1345-1348

[3] Z.Muskalski, S.Wiewiorowska, Procedia Manuf.2015, 2, 181-185

[4] S.David, https://sciencing.com/mechanical-properties-mild-steel-6618717.html.14 March 2018

[5] A. A.Al-Amiery, F. A. B. Kassim, A. A. H.Kadhum, A. B. Mohamad, Sci. Rep., 2016, 6, 1-13

[6] L. O. Olasunkanmi, I. B. Obot, M. M. Kabanda, E. E. Ebenso, J. Phys. Chem. C2015, 119, 16004−16019

[7] W.Zhang, H. J. Li, Y.Wang, Y. Liu, Q. Z. Gua, Y. C. Wu, New J. Chem., 2018,42, 12649-12665

[8] A. K. Singh, S. Thakur, B. Pani, G. Singh, New J. Chem.2018,42, 2113-2124

[9] R. Rosa, C. Ponzoni, C. Leonelli, Inorganics, 2014, 2, 191-210

[10] G. R. Qu, L. Zhao, D. C. Wang, J. Wua, H. M. Guo, Green Chem.2008,10, 287-289

[11] O. B.Locos,C. C.Heindl,A.Corral,M. O.Senge,E. M.Scanlan, Eur. J. Org. Chem.2010, 1026–1028

[12] S. E.Harpstrite,S. D.Collins,A.Oksman,D. E.Goldberg,V.Sharma, Med. Chem.2008, 4, 392-395

[13] W. A.Zoubi,A. A. S.Al-Hamdani,I. P.Widiantara,R. G.Hamoodah,Y. G.Ko, J Phys Org Chem.2017, 30, e3707, 1-12

[14] S. K.Bharti,G.Nath,R.Tilak,S. K.Singh, Eur. J. Med. Chem., 2010, 45, 651-660

[15] Z. D.Mou,N.Deng,F.Zhang,J.Zhang,J.Cen,X.Zhang, Eur J Med Chem.2017, 138, 72-82

[16] A. K. Singh, P. Singh, J. Ind. Eng. Chem. 2015, 21, 552-560

[17] W. Y.Wong,X. Z.Wang,Z.He,K. K.Chan,A. B.Djurisic,K. Y.Cheung,C. T.Yip, A. M.Ching,Y. Y.Xi,C. S. K.Mak,W. K.Chan, J. Am. Chem. Soc. 2007, 129, 14372−14380

[18] F.Zhang,B.Sun,T.Song,X.Zhu,S.Lee, Chem. Mater. 2011, 23, 2084−2090

[19] T.Ghosh,J. S.Panicker,V. C.Nair, Polymers2017, 9, 112−151

[20] K. Sztanke, A. Maziarka, A. Osinka, M.Sztanke, An insight into synthetic Schiff bases revealing anti proliferative activities in vitro. Bioorg. Med. Chem. **2013**, 21, 3648−3666

[21] K. M.Raj, B. Vivekananda, G. Y. Nagesh, B. H. M. Mruthyunjayaswamy,J. Mol. Struct. 2014, 1059, 280−293

[22] A. K. Singh, S. Shukla, I. Ahamad, M. A. Quraishi, J. Heterocycl. Chem. 2009, 46, 571-574

[23] P. Singh, D. P. Singh, K. Tiwari, M. Mishra, A. K. Singh, V. P. Singh, RSC Adv. 2015, 5, 45217-45230

[24] A. K. Singh, S. Thakur, B. Pani, E. E. Ebenso, M. A. Quraishi, A. K. Pandey, ACS Omega,2018, 3, 4695-4705

[25] B. Delley, J. Chem. Phys. 2000, 113, 7756–7764

[26] Materials Studio, Revision 6.0, Accelrys Inc., San Diego, USA, 2013

[27] J. P.Perdew,K. Burke, Y. Wang,Phys. Rev. B.1996, 54, 16533

[28] R. S. Mulliken, J. Chem. Phys. 1955, 23, 1833–1840

[29] M. J. Dewar, W. Thiel,J. Am. Chem. Soc.1977, 99, 4899–4907

[30] R. G. Pearson,Coord. Chem. Rev. 1990, 100, 403–425

[31] S. Martinez,Mater. Chem. Phys.2003, 77, 97–102

[32] Z. Cao, Y. Tang, H. Cang, J. Xu, G. Lu, W. Jing, Corros. Sci.2014, 83, 292–298

[33] S. K. Saha, M. Murmu, N. C. Murmu, P. Banerjee, J. Mol. Liq. 2016, 224, 629–638

[34] R. G. Parr, W. Yang, J. Am. Chem. Soc. 1984, 106, 4049–4050

[35] R.R.Contreras, P. Fuentealba, M. Galvan, P. Perez, Chem. Phys. Lett. 1999, 304, 405–413

[36] H. Sun, J. Phys. Chem. B. 1998, 102, 7338–7364

[37] S. K. Saha, A. Dutta, P. Ghosh, D. Sukul, P. Banerjee, Phys. Chem. Chem. Phys. 2016, 18, 17898–17911

[38] A. K. Singh, M. A. Quraishi,Corros. Sci. 2010, 52, 152-160

[39] A. S. Fouda, M. Abdallah, Z. El-Badrawy, Affr. J. P. Appl. Chem. 2011, 5, 224-236

[40] S. K. Saha, A. Dutta, P. Ghosh, D.Sukul, P. Banerjee, PhysChemChem Phys.2016, 17, 17898-17911

[41] S. B. Aoun, RSC Adv., 2017, 7, 36688-3696

[42] S. Zhang, Entropy: A concept that is not a physical quantity, Physics Essays, June 2012; DOI 10.4006/0836-1398-25.2.172

[43] R. T. Loto, C.AkintoyeLoto, O. Joseph, G. Olanrewaju, Results Phys. 2016, 6, 305–314

[44] A. Karimi, I. Danaee, H. Eskandari, M. RashvanAvei, J. Cent. South Univ. 2016, 23, 249−257

[45] M.Yadav, D. Behera, S. Kumar, R. R. Sinha, Ind. Eng. Chem. Res. 2013, 52, 6318-6328

[46] J. D. Talati, D. K. Gandhi, Corros. Sci. 1983, 23, 1315-1332

[47] Z. Szklarska-Smialowska, J. Mankowski, Corros. Sci.1978, 18, 953-960

[48] X. Zheng, M. Gong, Q. Li, L. Guo,Sci. rep. 2018 DOI: 10.1038/s41598-018-27257-9

[49] A. K. Singh, M. A. Quraishi, Corros. Sci., 2009, 51, 2752-2760

[50] S. John, A. Joseph, Mater. Corros. 2013, 64, 625-632

[51] M. Das, A. Biswas, B. K. Kundu, S. M. Mobin, G. Udayabhanu, S. Mukhopadhyay, RSC Adv. 2017, 7, 48569-48585

[52] M. Farsak, A. O. Yuce, G. Kardas, ChemistrySelect 2017, 2, 3676 – 3682

[53] P. B. Raja, M.Fadaeinasab, A. K. Qureshi, A. A. Rahim, H. Osman, M. Litaudon, K. Awang, Ind. Eng. Chem. Res.2013, 52, 10582–10593

[54] D. K. Patel, S. Senapati, P. Mourya, M. M. Singh, V. K. Aswal, B. Ray, P. Maiti, ACS Biomater. Sci. Eng.2017, 3, 3351–3363

[55] E.S. Ferreira, C. Giancomlli, F.C. Giacomlli, A. Spinelli, Mater. Chem. Phys., 83 (2004) 129–134

[56] M. M. Solomon, S. A.Umoren, I. B. Obot, A. A. Sorour, H. Gerengi, ACS Appl. Mater. Interfaces, DOI: 10.1021/acsami.8b09487

[57] M. Yadav, D. Behera, S. Kumar, R. R. Sinha, Ind. Eng. Chem. Res. 2013, 52, 6318–6328

[58] R. N. Singh, A. Kumar, R. K. Tiwari, P. Rawat, Spectrochim. Acta. A. Mol. Biomol. Spectrosc.2013, 112, 182–190. doi:10.1016/j.saa.2013.04.002

[59] S. K. Saha, P. Ghosh, A. Hens, N. C. Murmu, P. Banerjee, Phys. E Low-Dimens. Syst. Nanostructures2015, 66, 332–341

[60] M. Lebrini, M. Lagrenee, H. Vezin, M. Traisnel, F. Bentiss, Corros. Sci.2007, 49, 2254–2269

[61] N. A. Wazzan, J. Ind. Eng. Chem.2015, 26, 291–308

[62] A. Kokalj, Electrochim Act.2010, 56, 745–755

[63] H. Lgaz, K. S. Bhat, R. Salghi, S. Jodeh, M. Algarra, B. Hammouti, I. H. Ali, A. Essamri, J. Mol. Liq.2017, 238, 71–83

[64] A. Singh, K. R. Ansari, J. Haque, P. Dohare, H. Lgaz, R. Salghi, M. A. Quraishi, J. Taiwan Inst. Chem. Eng.2018, 82, 233–251

[65] H. Lgaz, R. Salghi, K. S. Bhat, A. C. Shubhalaxmi, S. Jodeh, J. Mol. Liq. 2017, 244, 154–168

[66] J. Zhou, S. Chen, L. Zhang, Y. Feng, H. Zhai, J. Electroanal. Chem.2008, 612, 257–268

[67] A. Kokalj, Corros. Sci.2013, 70, 294–297

[68] A. Liu, X. Ren, J. Zhang, C. Wang, P. Yang, J. Zhang, M. An, D. Higgins, Q. Li, G. Wu, RSC Adv. 2014, 4, 40606–40616

Fig. 1 Schematic representation of synthesis of all the studied inhibitors and chemical structure of all the inhibitors

Fig. 2 (a) IR spectra of all the four studied compounds, (b) IR spectra of the film removed from the surface of electrode dipped in solution of different inhibitors and (c) ^{1}H NMR spectra of all the four studied inhibitors

Fig. 3 Variation of corrosion rate against the concentration of different inhibitors

Fig. 4 (a) Plot of log C_R vs. 1/T, (b) Plot of log C_R/T vs. 1/T (c) Langmuir adsorption isotherm for the adsorption of different inhibitors on the mild steel surface and (d) adsorption isotherm plot for ln K_{ads}*vs.* 1/T

Fig. 5 (a) Effect of the presence of 400 mg $L^{-1}$of all the studied inhibitors in 0.5 M H_2SO_4 solution on Nyquist plots, (b) Effect of the presence of 400 mg $L^{-1}$of all the studied inhibitors in 0.5 M H_2SO_4 solution on Bode plots, (c) Effect of the presence of 400 mg $L^{-1}$of all the studied inhibitors in 0.5 M H_2SO_4 solution on Nyquist plots and (d) Experimental and fitted data obtained for 1 M HCl solution and (e) Equivalent circuit used to analyze the experimental data

Fig. 6 Effect of the presence of studied inhibitors on potentiodynamic polarization curves of mild steel in 0.5 M H_2SO_4

Fig. 7 Scanning electron micrograph and EDX spectrum of mild steel immersed in (a&a*) 0.5 M H_2SO_4, (b& b*) 0.5 M H_2SO_4 + 400 mg L^{-1} of ATBH, (c& c*) 0.5 M H_2SO_4 + 400 mg L^{-1} of PTBH, (d& d*) 0.5 M H_2SO_4 + 400 mg L^{-1} of ATABH and (e& e*) 0.5 M H_2SO_4 + 400 mg L^{-1} of PTABH

Fig. 8 Atomic force micrograph of mild steel immersed in (a) 0.5 M H_2SO_4, (b) 0.5 M H_2SO_4 + 400 mg L^{-1} of ATBH, (c) 0.5 M H_2SO_4 + 400 mg L^{-1} of PTBH, (d) 0.5 M H_2SO_4 + 400 mg L^{-1} of ATABH and (e) 0.5 M H_2SO_4 + 400 mg L^{-1} of PTABH

Fig. 9 XPS spectra of mild steel surface removed after immersion in 0.5 M H_2SO_4 with 400 mg L^{-1} of ATBH: (a) survey scan spectra, (b) narrow scan spectra of S, (c) C, (d) N, (e) O and (f) Fe

Fig. 10 Variation of contact angle of electrode surface with concentration of different electrolytic solutions

Fig. 11 Optimized structures, HOMOs and LUMOs of ATBH, ATABH, PTBH and PTABH

Fig. 12 Side views and top views of the model structures simulating the adsorption of ATBH, ATABH, PTBH and PTABH on the FE (110) surfaces

Table 1 Yield and physical data of the studied inhibitors

Name of Inhibitor	Time Taken in Synthesis (Min.)		Yield (%)		M.P. (°C)	I.R. (ν cm^{-1}, KBr)
	Con.	M.W.	Con.	M.W.		
ATBH	240	3.5	68	92	182	ν(NH) 3330 m; ν(CH_3) 3079w; ν(C=O) 1647 m; ν(C=N) 1573m; ν(N–N) 998w
PTBH	280	4.0	65	90	130	ν(NH) 3366 m; ν(CH_3) 3079w; ν(C=O) 1650 m; ν(C=N) 1550m; ν(N–N) 995w
ATABH	230	3.0	70	93	124	ν(NH_2) 3469 m; ν(NH) 3358 m; ν(C=O) 1630 m; ν(C=N) 1570m; ν(N–N) 980w
PTABH	240	3.0	67	90	116	ν(NH_2) 3470 m; ν(NH) 3370 m; ν(C=O) 1640 m; ν(C=N) 1580m; ν(N–N) 1000w

^{1}H NMR (DMSO-d_6; δ ppm)

ATBH: 2.367 (s, 3H,CH_3); 10.76 (s, 1H, NH); 7.596–7.473(m, 5H, Ar–H); 7.847 (d,2H, J = 6.3 Hz, thiophene moiety); 7.096 (t, 1H, J = 3.6, thiophene moiety)

PTBH: 2.75 (d, 2H, CH_2); 1.09 (d, 3H, CH_3); 7.59-7.40 (m, 4H, Ar-H); 10.76 (s, 1H, NH); 7.89 (s, 2H, thiophene moiety); 7.07 (s, 1H, thiophene moiety)

ATABH: 2.32 (s, 3H, CH_3); 6.18 (s, 2H, NH_2); 10.47 (s, 1H, NH); 7.16 (d, 1H, Thiophene moiety); 7.13 (t, 1H, Thiophene moiety); 7.51 (d, 1H, Thiophene moiety); 6.54 (m, 1H, Ar-H); 7.64 (d, 1H, Ar-H); 6.72 (d, 1H, Ar-H); 7.08 (m, 1H, Ar-H)

PTABH: 2.86 (m, 2H, CH_2); 1.10 (dd, 3H, CH_3); 10.55 (s, 1H, NH); 6.10 (s, 2H, NH_2); 6.72 (t, 1H, Ar-H); 6.51 (m, 1H, Ar-H); 7.50 (m, 1H, Ar-H); 7.15 (m, 1H, Thiophene moiety); 7.37 (m, 2H, Thiophene moiety); 7.06

CHN (%)

ATBH: C = 63.81; H = 4.97; N = 11.45

PTBH: C = 65.12; H = 5.44; N = 10.80

ATABH: C = 60.32; H = 5.02; N = 16.12

PTABH: C = 61.55; H = 5.50; N = 15.33

(m, 1H, Thiophene moiety)

Table 2 Activation parameters for mild steel corrosion in 0.5 M H_2SO_4 in the absence and presence of all the four studied inhibitors ATBH, PTBH, ATABH and PTABH

Name of Inhibitor	E_a (kJ mol^{-1})	λ(mgcm^{-2})	
ΔH^* (kJmol^{-1})	ΔS^* (JK^{-1}mol^{-1})		
-	37.0	1.99×10^7	34.4
-114.0			
ATBH	52.9	1.02×10^9	50.3
-81.3			
PTBH	55.1	1.86×10^9	52.5
-76.3			
ATABH	56.5	2.63×10^9	53.9
-73.4			
PTABH	66.4	6.00×10^{10}	63.8
-47.5			

Table 3 Thermodynamic Adsorption Parameters for adsorption of ATBH, PTBH, ATABH and PTABH on Mild Steel in 0.5 M H_2SO_4

Name of Inhibitor	Temperature (K)	K_{ads} ($10^3 \times$ M^{-1})	$-\Delta G^0_{ads}$ (kJmol^{-1})
ΔH^0_{ads} (kJmol^{-1})	ΔS^0_{ads} (JK^{-1}mol^{-1})		
ATBH	303	1.43	28.4
-31.5	198.6		
	313	2.80	31.1
	323	3.62	32.8
	333	4.55	35.0
PTBH	303	1.75	28.9
-33.3	206.4		
	313	3.74	31.9
	323	4.47	33.4
			333
6.14	35.8		
ATABH	303	1.96	29.2
-34.9	213.1		
	313	4.49	32.3
	323	5.57	33.9
	333	7.24	36.3
PTABH	303	2.46	29.8
-41.3	235.4		
	313	5.52	32.9

323	7.64	34.8
333	11.3	37.5

Table 4 Impedance Parameters for Mild Steel in 0.5 M H_2SO_4in the absence and presence of different concentrations of all the studied inhibitors

Name of Inhibitor	Conc. of Inhibitor	R_s	R_{ct}	Y_0	n	C_{dl}	P_{EIS} %
	(mg L^{-1})	(Ωcm^2)	(Ωcm^2)	($10^{-6}\Omega^{-1}$ cm^{-2})		(μF cm^{-2})	
	-	1.2	46.8	257.6	0.833	106.6	-
ATBH	50	0.9	151.2	120.4	0.834	54.2	69.0
	100	1.2	262.3	106.2	0.836	52.6	82.1
	200	0.8	342.1	90.6	0.841	47.0	86.3
	300	1.1	400.6	82.5	0.845	44.1	88.3
	400	1.1	470.5	73.5	0.863	43.1	90.0
PTBH	50	1.1	171.0	112.4	0.836	51.8	72.6
	100	0.9	313.1	98.8	0.839	51.0	85.0
	200	1.1	381.5	82.1	0.843	45.4	87.7
	300	1.0	482.7	71.7	0.848	39.3	90.3
	400	1.0	644.8	61.7	0.864	37.1	92.7
ATABH	50	1.0	186.3	110.2	0.838	52.0	74.8
	100	0.8	369.4	94.1	0.841	49.8	87.3
	200	1.0	437.2	80.2	0.846	43.6	89.3
	300	0.9	582.2	68.7	0.862	41.0	91.9
	400	1.2	737.8	49.0	0.885	31.8	93.7
PTABH	50	1.1	215.1	91.3	0.838	42.8	78.2
	100	0.9	425.9	78.0	0.843	41.4	89.0
	200	1.2	587.4	62.2	0.849	34.8	92.0
	300	1.1	851.8	38.9	0.867	23.0	94.5
	400	1.9	1264.1	10.9	0.886	6.3	96.3

Table 5 Potentiodynamic polarization parameters for mild steel in the absence and presence of different concentrations of all the four studied inhibitors in 0.5 M H_2SO_4

Name of Inhibitor	Conc. of Inhibitor (mg L^{-1})	$-E_{corr}$ (mV *vs.* SCE)	i_{corr} (μA cm^{-2})	βa (mV dec^{-1})	$-\beta$c (mV dec^{-1})	P_{PDP} %
-	-	446	1770	91.2	154.5	-
ATBH	50	464	589	65.4	144.4	66.7
	100	476	372	68.5		169.0
		78.9				
	200	438	281	67.1	134.8	84.1
	300	510	210	130.5		149.1
		88.1				
	400	484	196	77.9		127.3
		88.9				
PTBH	50	466	489	66.2	160.1	72.4
	100	475	269	66.0		175.6
		84.8				
	200	480	230	72.9	178.9	87.0
	300	495	188	75.6		154.3
		89.4				
	400	480	160	68.2		158.1
		90.9				
ATABH	50	465	485	66.8	142.8	73.7
	100	456	268	70.3	182.1	84.8
	200	466	198	77.7		145.2
		88.8				
	300	478	174	71.3		146.7
		90.1				
	400	486	123	63.4		151.1
		93.0				
PTABH	50	446	429	78.1	171.0	75.8
	100	496	246	80.4	122.2	86.1
	200	469	176	83.9		148.2
		90.0				
	300	499	142	96.1		145.2
		92.0				

	400	487	95	61.3
	141.8	94.6		

Name of Inhibitor	Conc. of Inhibitor (mg L^{-1})	Inhibition efficiency (E%)		
		E_{WL} %	E_{EIS} %	E_{PDP} %
ATBH	50	70.1	69.0	66.7
	100	82.1	82.1	78.9
	200	85.6	86.3	84.1
	300	88.2	88.3	88.1
	400	90.1	90.0	88.9
PTBH	50	73.1	72.6	72.4
	100	85.3	85.0	84.8
	200	87.4	85.7	87.0
	300	90.5	90.3	89.4
	400	92.6	92.7	90.9
ATABH	50	75.2	74.8	73.7
	100	87.4	87.3	84.8
	200	89.6	89.3	88.8
	300	91.8	91.9	90.1
	400	93.9	93.7	93.0
PTABH	50	78.3	78.2	75.8
	100	89.0	89.0	86.1
	200	91.8	92.0	90.0
	300	94.3	94.5	92.0
	400	97.2	96.3	94.6

Table 7 Quantum chemical parameters of compounds ATBH, PTBH, ATABH and PTABH

Parameter	ATBH	ATABH	PTBH	PTABH
E_{HOMO} (eV)	-5.013	-4.465	-4.485	-4.390
E_{LUMO} (eV)	-2.207	-1.729	-1.744	-1.739
ΔE (eV)	2.806	2.736	2.741	2.651
ΔN	0.43	0.63	0.62	0.66

Table 8 Fukui indices for the nucleophilic and electrophilic attacks of inhibitor molecules calculated using DFT method

PTBH	f_k^+	f_k^-		PTABH		f_k^+	f_k^-	ATABH	f_k^+	f_k^-
	ATBH		f_k^+		f_k^-					
C(1)	0.048	0.057		C(1)		0.050	0.054	C(1)	0.063	
0.024	C(1)		0.051		0.056					
S(2)	**0.092**	**0.113**		S(2)		**0.104**	**0.100**	S(2)	**0.144**	
0.041	S(2)		**0.110**		**0.107**					
C(3)	-0.006	0.032		C(3)		-0.003	0.025	C(3)	0.005	-
0.007	C(3)		-0.002		0.023					
C(4)	0.047	0.038		C(4)		0.049	0.037	C(4)	0.061	
0.019	C(4)		0.048		0.039					
C (5)	0.009	0.036		C(5)		0.010	0.031	C(5)	0.013	
0.011	C(5)		0.010		0.033					
C(6)	0.061	0.047		C(6)		0.068	0.042	C(6)	0.068	
0.025	C(6)		0.059		0.038					
C(7)	-0.020	-0.029		C(7)		-0.025	-0.023	C(7)	-0.022	-
0.005	C(7)		-0.021		-0.010					
N(8)	0.049	0.058		N(8)		0.057	0.051	N(8)	0.088	
0.027	N(8)		0.059		0.077					
N(9)	-0.002	-0.054		N(9)		0.000	0.047	N(9)	-0.006	
0.033	N(9)		0.001		0.052					
C(10)	0.056	0.021		C(10)		0.051	0.017	C(10)	0.024	
0.006	C(10)		0.046		0.019					
O(11)	0.079	0.070		O(11)		0.071	0.065	O(11)	0.032	
0.029	O(11)		0.058		0.071					
C(18)	0.004	-0.013		C(18)		-0.004	-0.006	C(19)	-0.007	
0.047	C(19)		0.005		-0.011					
C(19)	0.021	0.008		C(19)		0.019	0.007	C(20)	0.011	
0.013	C(20)		0.019		0.009					
C(20)	0.008	0.007		C(20)		0.006	0.015	C(21)	0.008	
0.038	C(21)		0.009		0.007					
C(21)	0.037	0.014		C(21)		0.0 28	0.013	C(22)	0.016	
0.012	C(22)		0.036		0.015					
C(22)	0.007	0.006		C(22)		0.008	0.010	C(23)	0.007	
0.056	C(23)		0.007		0.007					
C(23)	0.020	0.000		C(23)		0.017	0.013	C(24)	0.006	
0.010	C(24)		0.018		0.003					
C(29)	-0.011	-0.007		N(28)		-0.002	0.004	N(25)	0.005	
0.113										
				C(31)		-0.011	-0.007			

Table 9 Selected energy parameters obtained from MD simulations for adsorption of inhibitors on Fe (110) surface

System	$E_{\text{interaction}}$ (kJmol^{-1})	E_{binding} (kJmol^{-1})
Fe (110)/ATBH	-591.44	591.44
Fe(110)/ATABH	-659.09	659.09
Fe(110)/PTBH	-619.71	619.71
Fe(110)/PTABH	-673.12	673.12

Highlights

- All the thiophene based hydrazones were synthesized by microwave assisted method.
- Microwave-assisted solvent free synthesis was found economical and energy efficient.
- These inhibitors acted as mixed type but predominantly cathodic inhibitor.
- Their adsorption was investigated by XPS and IR spectrum.
- All the experimental results showed good agreement with DFT and MD study.

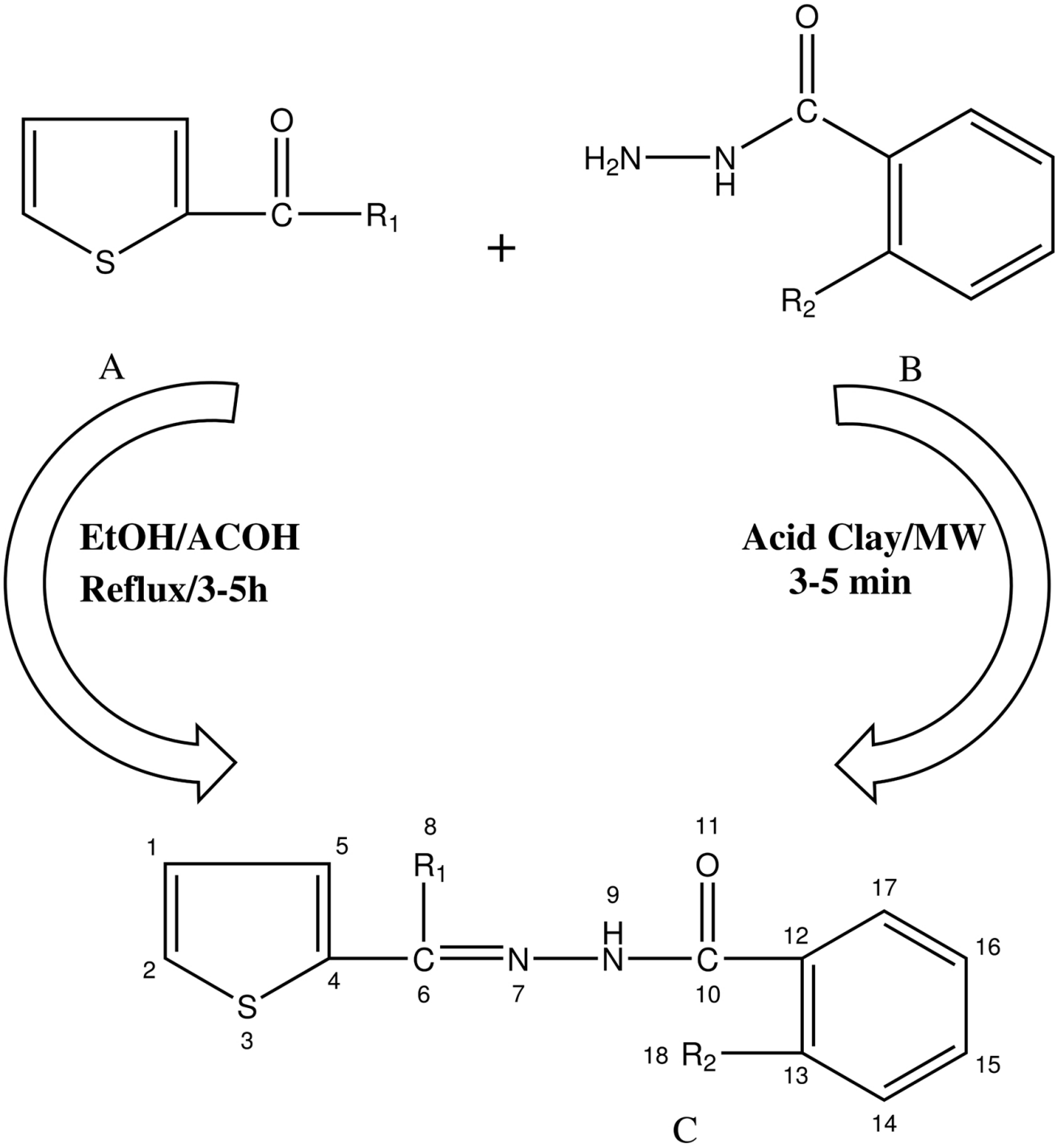

if R_1= CH_3, R_2= H; **ATBH**

if R_1= CH_2CH_3, R_2= H; **PTBH**

if R_1= CH_3, R_2= NH_2; **ATABH**

if R_1= CH_2CH_3, R_2= NH_2; **ATABH**

Figure 1

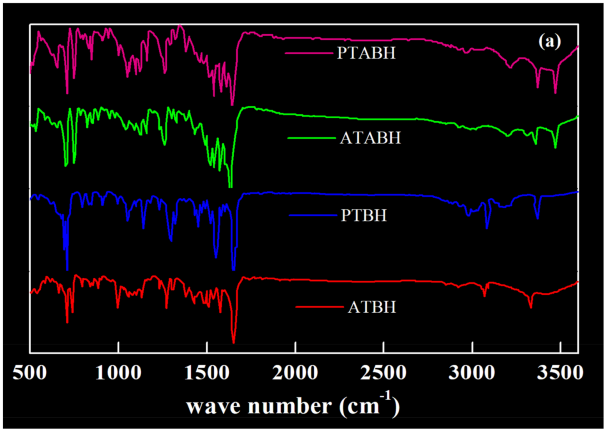
(a)
PTABH
ATABH
PTBH
ATBH
500
1000
1500
2000
2500
3000
3500
wave number (cm-1)

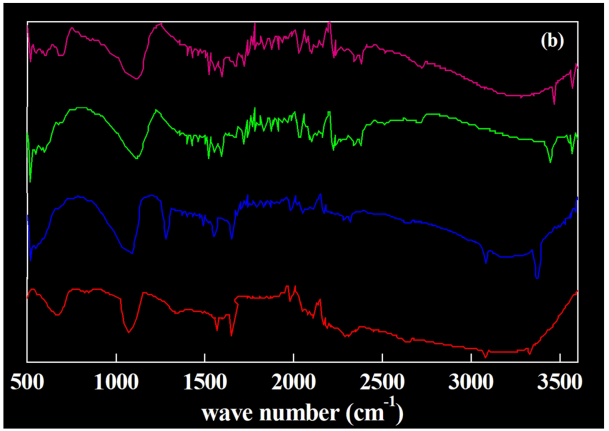
(b)
500
1000
1500
2000
2500
3000
3500
wave number (cm-1)

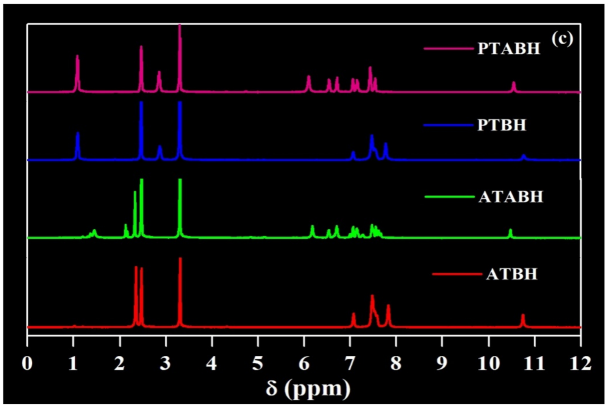
(c)
PTABH
PTBH
ATABH
ATBH
0
1
2
3
4
5
6
7
8
9
10
11
12
δ (ppm)

Figure 2

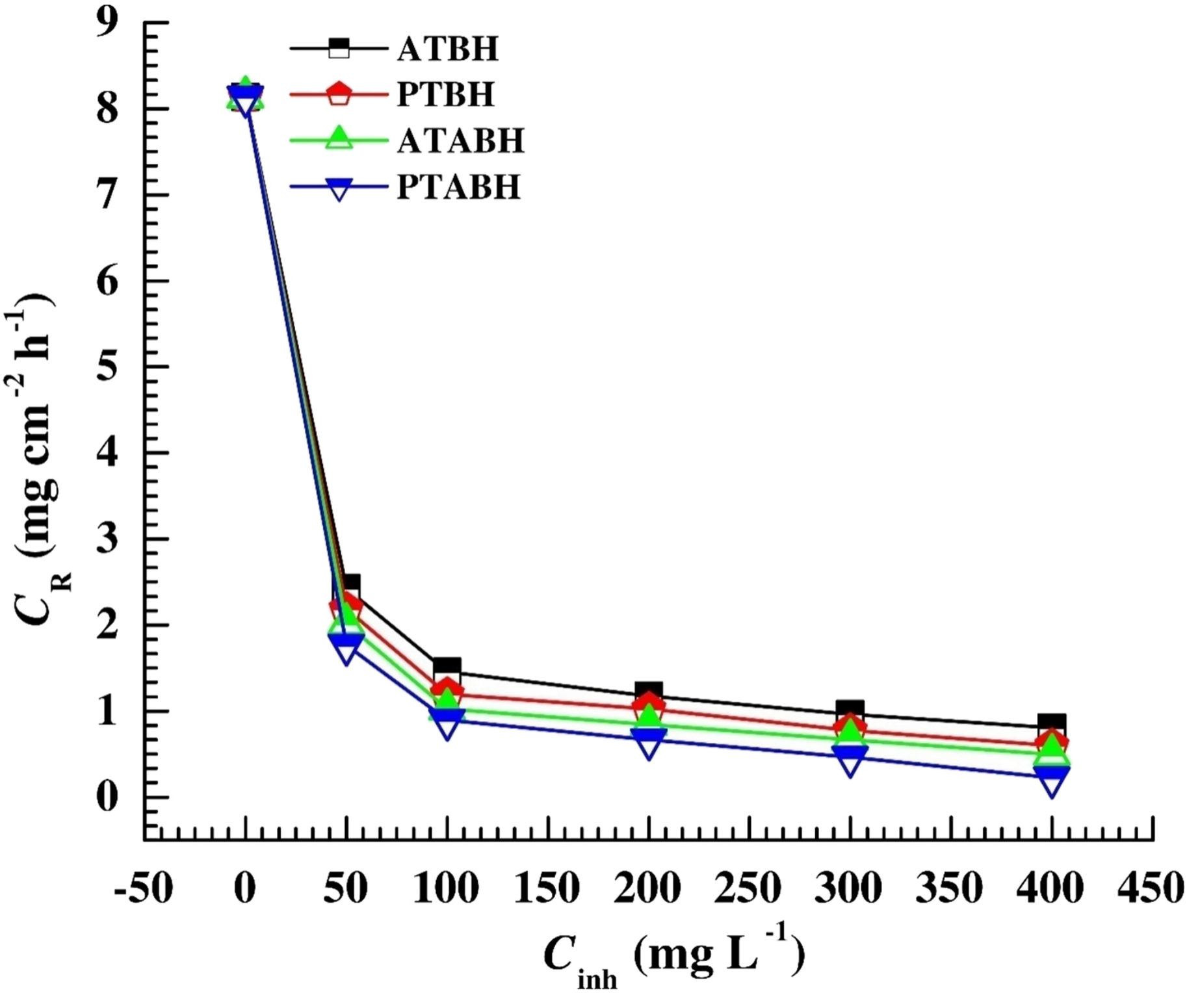
ATBH
PTBH
ATABH
PTABH
C_R (mg cm^{-2} h^{-1})
C_{inh} (mg L^{-1})
0
1
2
3
4
5
6
7
8
9
-50
0
50
100
150
200
250
300
350
400
450

Figure 3

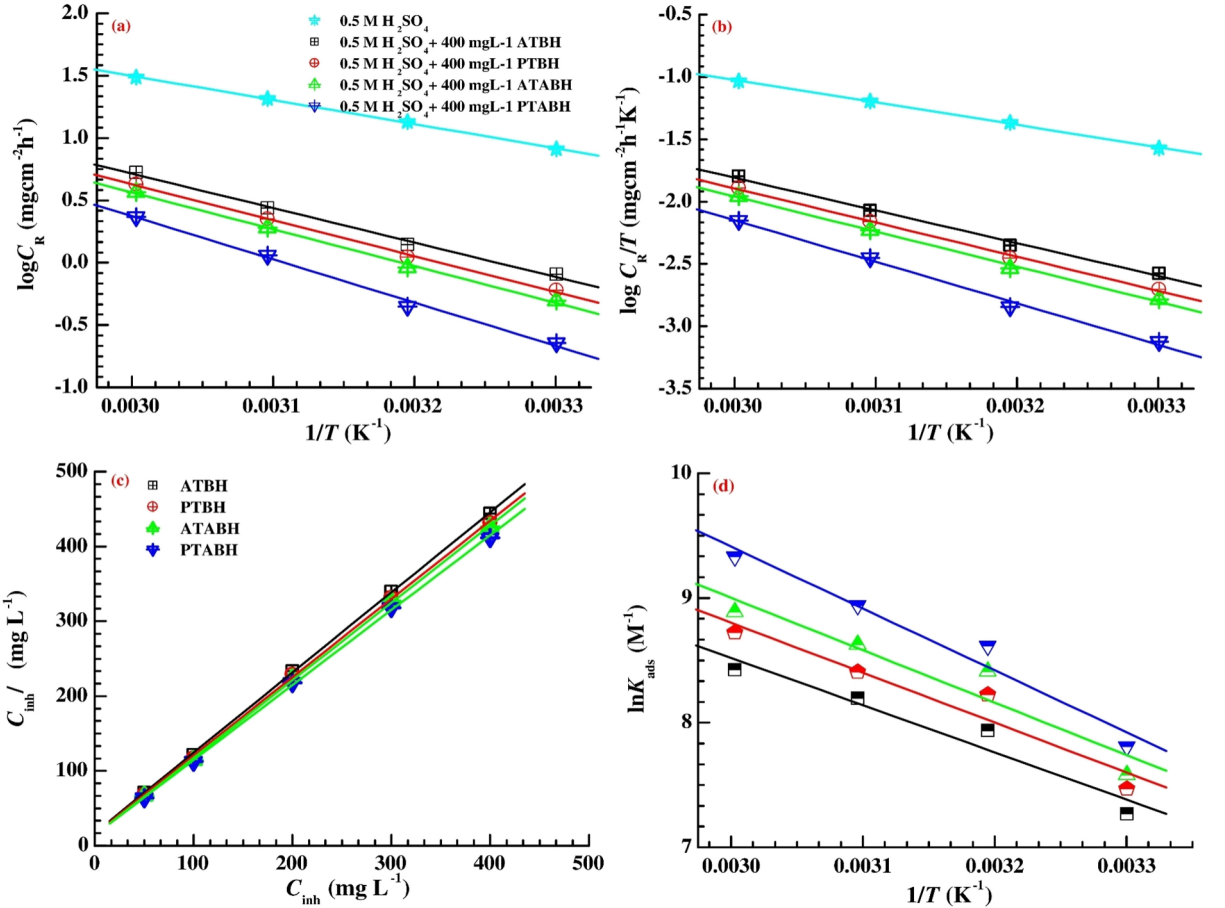
(a)
0.5 M H2SO4
0.5 M H2SO4+ 400 mgL-1 ATBH
0.5 M H2SO4+ 400 mgL-1 PTBH
0.5 M H2SO4+ 400 mgL-1 ATABH
0.5 M H2SO4+ 400 mgL-1 PTABH
logCR (mgcm-2h-1)
1/T (K-1)
(b)
log CR/T (mgcm-2h-1K-1)
1/T (K-1)
(c)
ATBH
PTBH
ATABH
PTABH
Cinh / (mg L-1)
Cinh (mg L-1)
(d)
lnKads (M-1)
1/T (K-1)

Figure 4

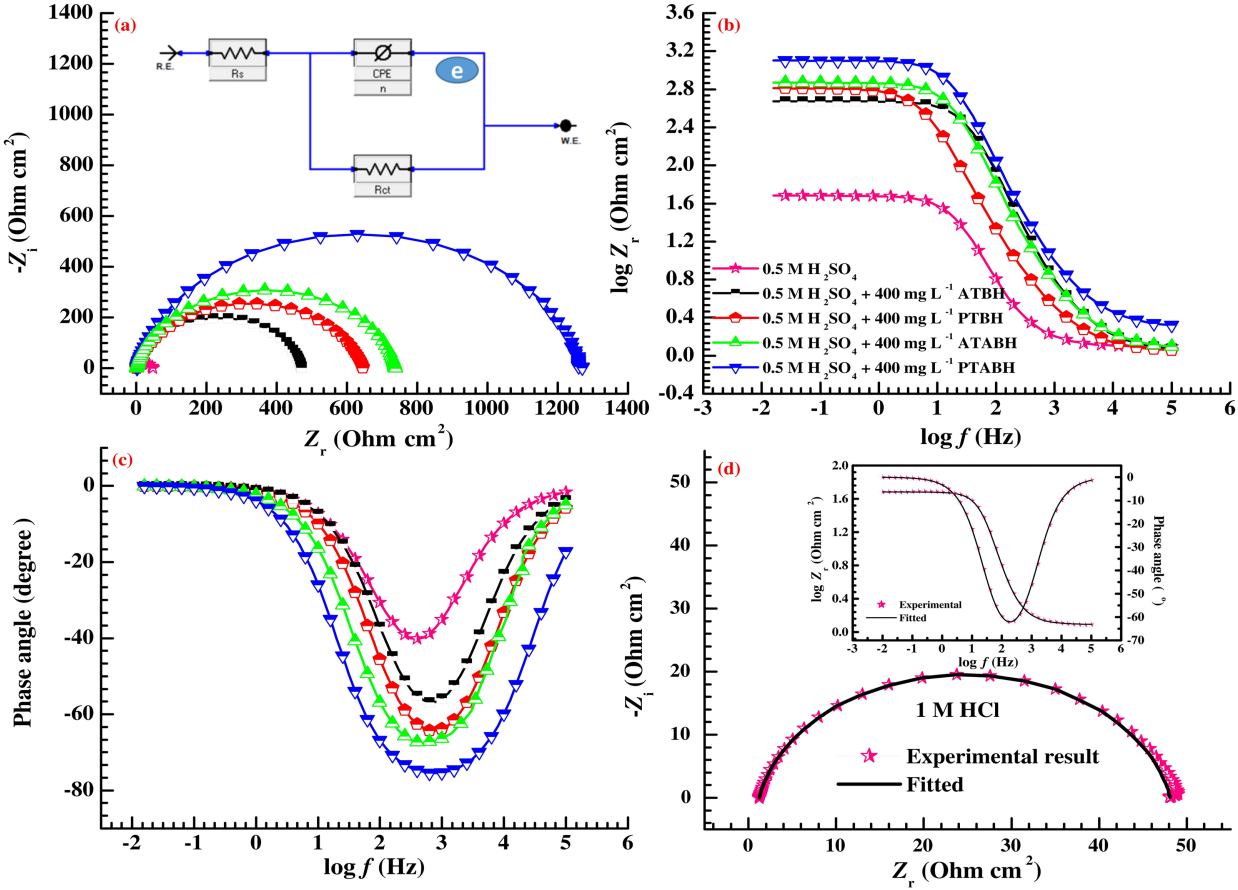
(a)
R.E.
Rs
CPE
n
e
W.E.
Rct
-Z_i (Ohm cm^2)
Z_r (Ohm cm^2)
(b)
log Z_r (Ohm cm^2)
log f (Hz)
0.5 M H2SO4
0.5 M H2SO4 + 400 mg L-1 ATBH
0.5 M H2SO4 + 400 mg L-1 PTBH
0.5 M H2SO4 + 400 mg L-1 ATABH
0.5 M H2SO4 + 400 mg L-1 PTABH
(c)
Phase angle (degree)
log f (Hz)
(d)
-Z_i (Ohm cm^2)
Z_r (Ohm cm^2)
log Z_r (Ohm cm^2)
Phase angle (°)
Experimental
Fitted
1 M HCl
Experimental result
Fitted

Figure 5

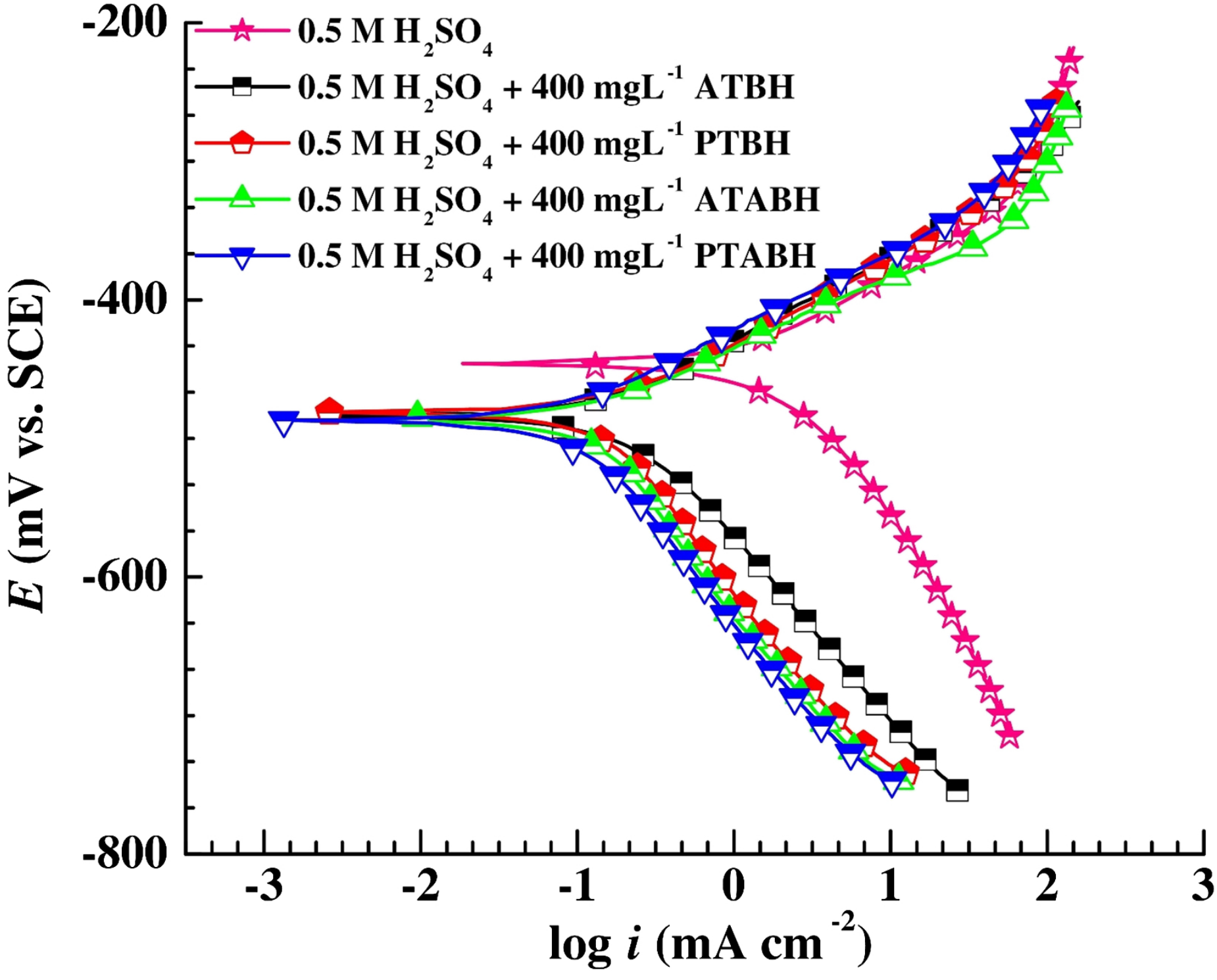
0.5 M H2SO4
0.5 M H2SO4 + 400 mgL-1 ATBH
0.5 M H2SO4 + 400 mgL-1 PTBH
0.5 M H2SO4 + 400 mgL-1 ATABH
0.5 M H2SO4 + 400 mgL-1 PTABH
E (mV vs. SCE)
-200
-400
-600
-800
-3
-2
-1
0
1
2
3
log i (mA cm-2)

Figure 6

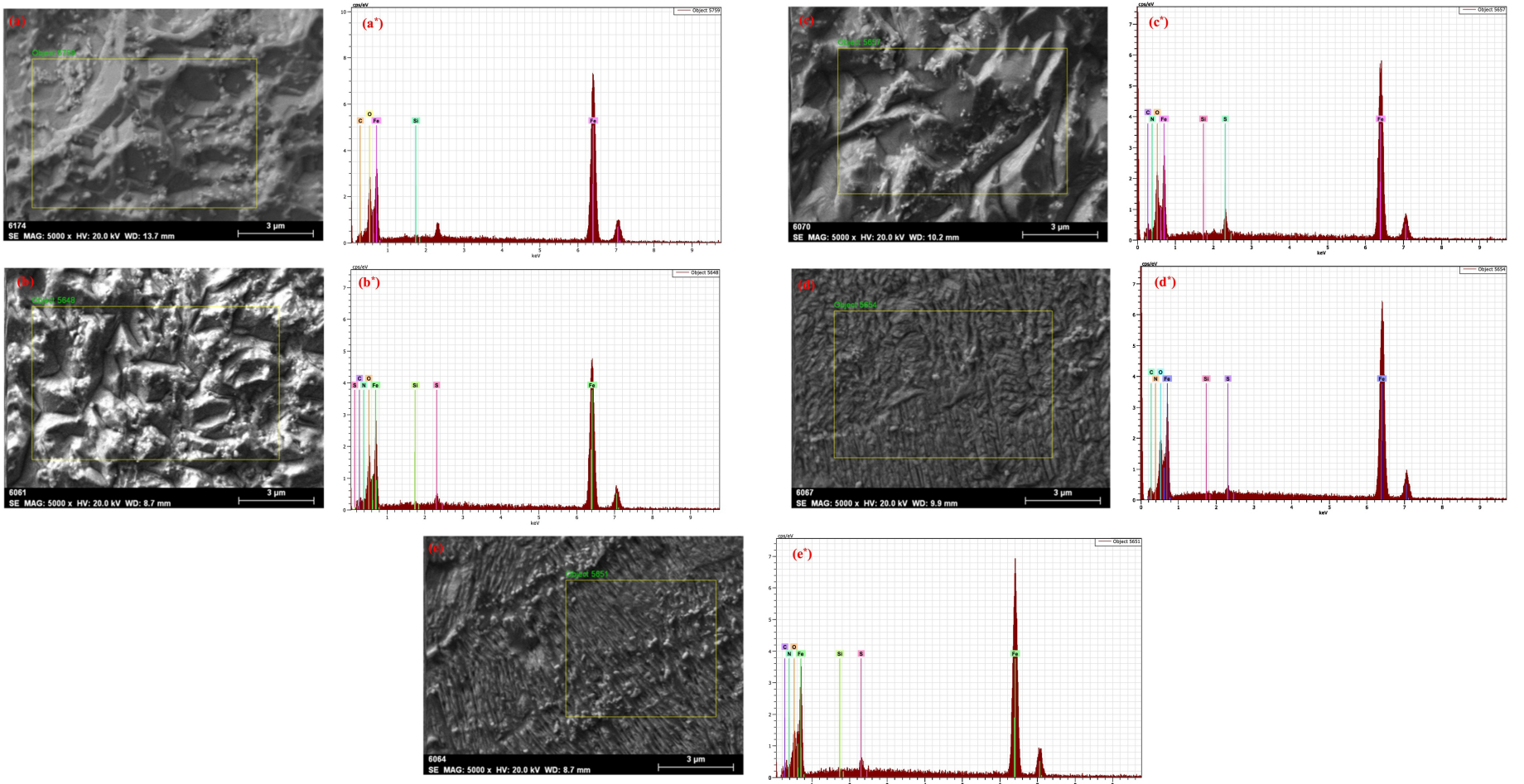
(a)
Object 5759
6174
SE MAG: 5000 x HV: 20.0 kV WD: 13.7 mm
3 µm
(a*)
cps/eV
Object 5759
C
O
Fe
Si
Fe
keV
(b)
Object 5648
6061
SE MAG: 5000 x HV: 20.0 kV WD: 8.7 mm
3 µm
(b*)
cps/eV
Object 5648
C
O
S
N
Fe
Si
S
Fe
keV
(c)
Object 5657
6070
SE MAG: 5000 x HV: 20.0 kV WD: 10.2 mm
3 µm
(c*)
cps/eV
Object 5657
C
O
N
Fe
Si
S
Fe
keV
(d)
Object 5654
6067
SE MAG: 5000 x HV: 20.0 kV WD: 9.9 mm
3 µm
(d*)
cps/eV
Object 5654
C
O
N
Fe
Si
S
Fe
keV
(e)
Object 5651
6064
SE MAG: 5000 x HV: 20.0 kV WD: 8.7 mm
3 µm
(e*)
cps/eV
Object 5651
C
O
N
Fe
Si
S
Fe
keV

Figure 7

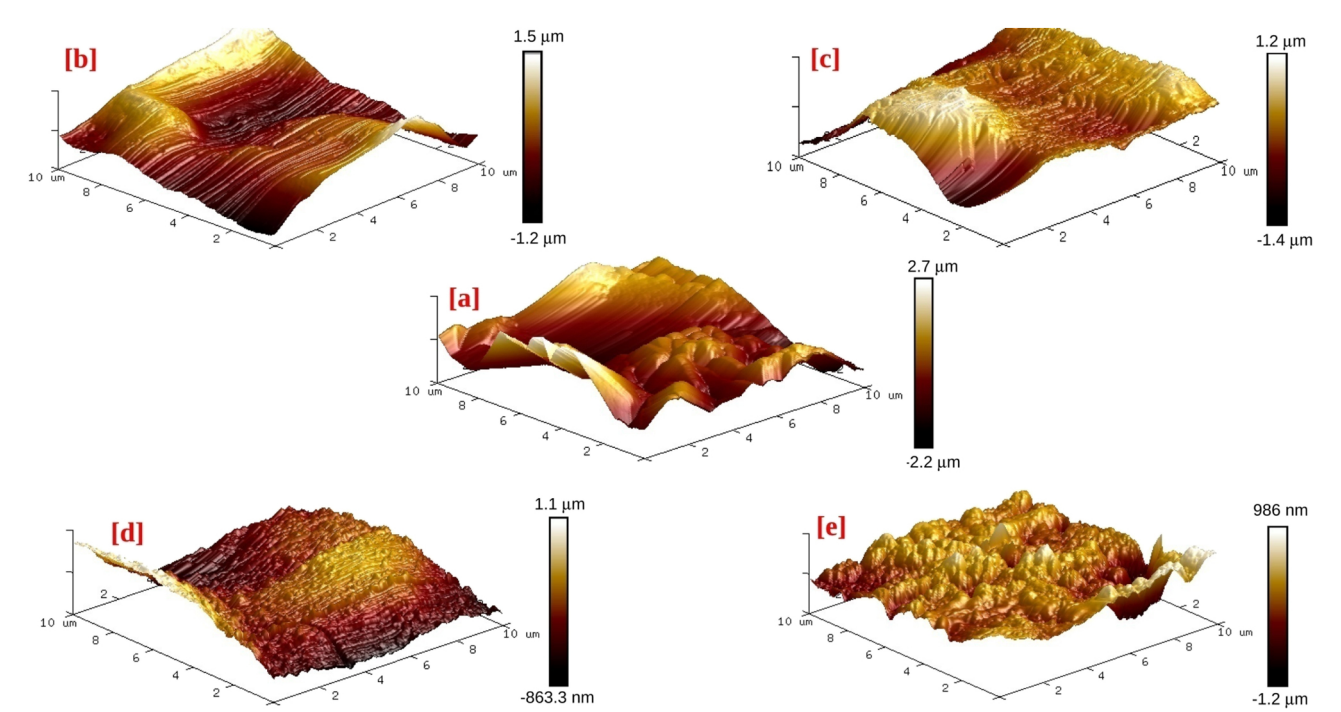
[b]
1.5 µm
-1.2 µm
[c]
1.2 µm
-1.4 µm
[a]
2.7 µm
-2.2 µm
[d]
1.1 µm
-863.3 nm
[e]
986 nm
-1.2 µm
10 um
2
4
6
8

Figure 8

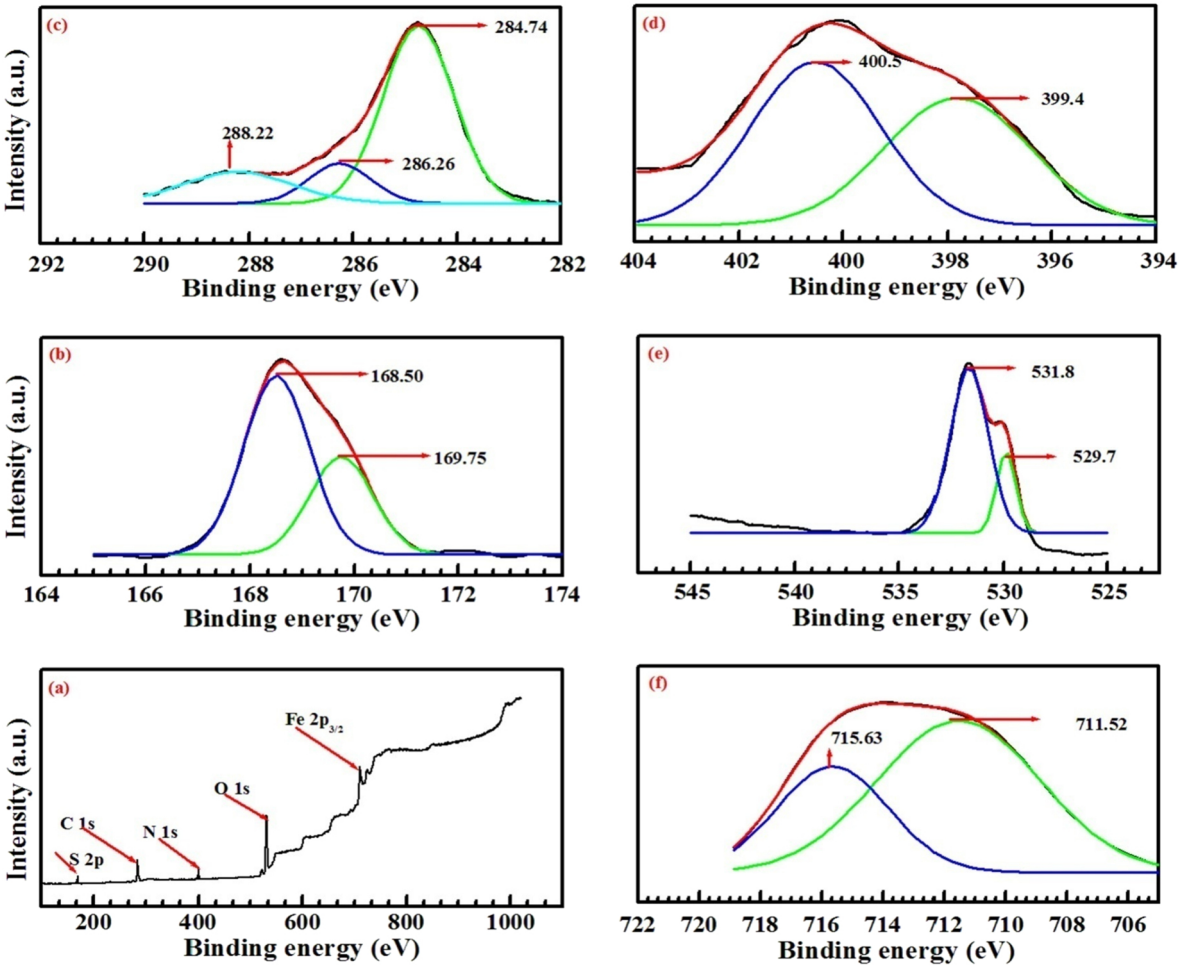
(c)
284.74
288.22
286.26
Intensity (a.u.)
292
290
288
286
284
282
Binding energy (eV)
(d)
400.5
399.4
404
402
400
398
396
394
Binding energy (eV)
(b)
168.50
169.75
Intensity (a.u.)
164
166
168
170
172
174
Binding energy (eV)
(e)
531.8
529.7
545
540
535
530
525
Binding energy (eV)
(a)
Fe 2p3/2
O 1s
C 1s
N 1s
S 2p
Intensity (a.u.)
200
400
600
800
1000
Binding energy (eV)
(f)
715.63
711.52
722
720
718
716
714
712
710
708
706
Binding energy (eV)

Figure 9

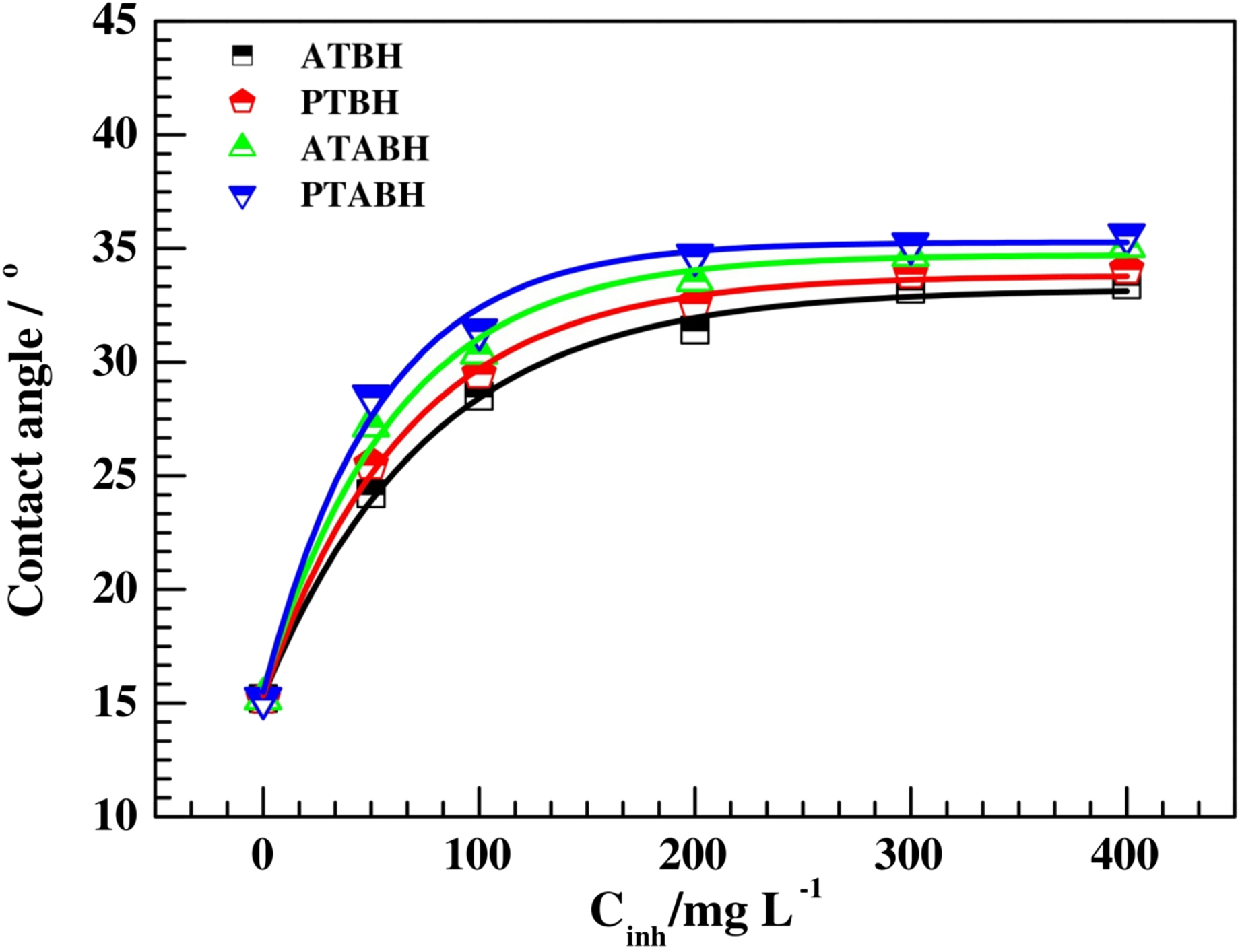
ATBH
PTBH
ATABH
PTABH
Contact angle / °
45
40
35
30
25
20
15
10
0
100
200
300
400
C inh /mg L -1

Figure 10

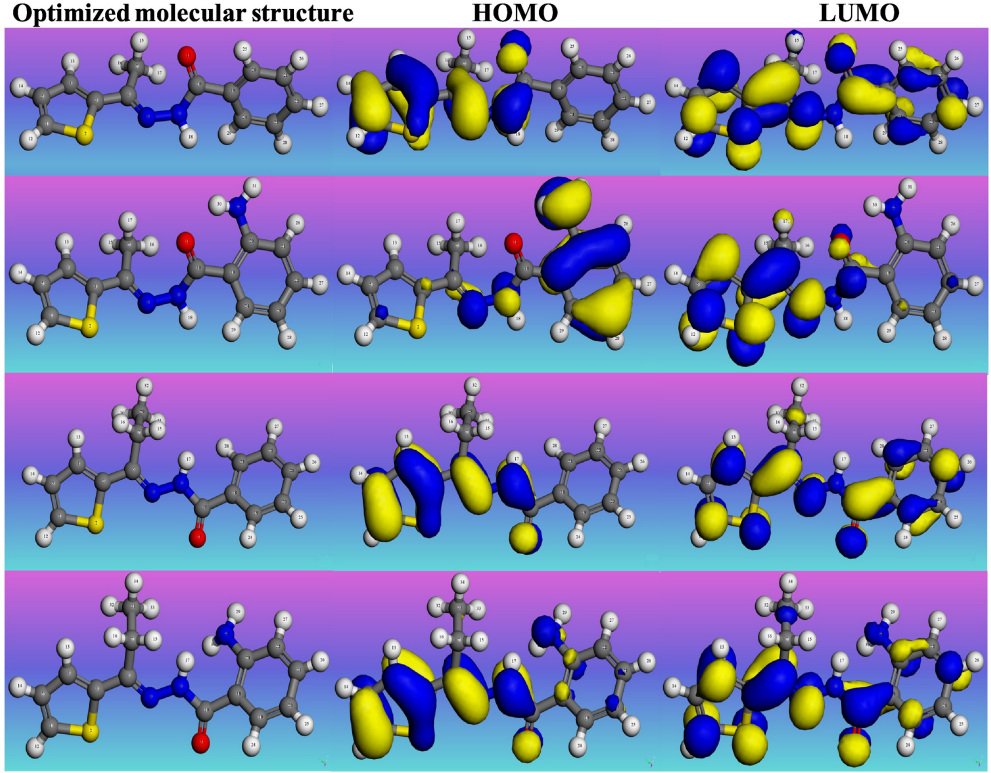
Optimized molecular structure
HOMO
LUMO
ATBH
ATABH
PTBH
PTABH

Figure 11

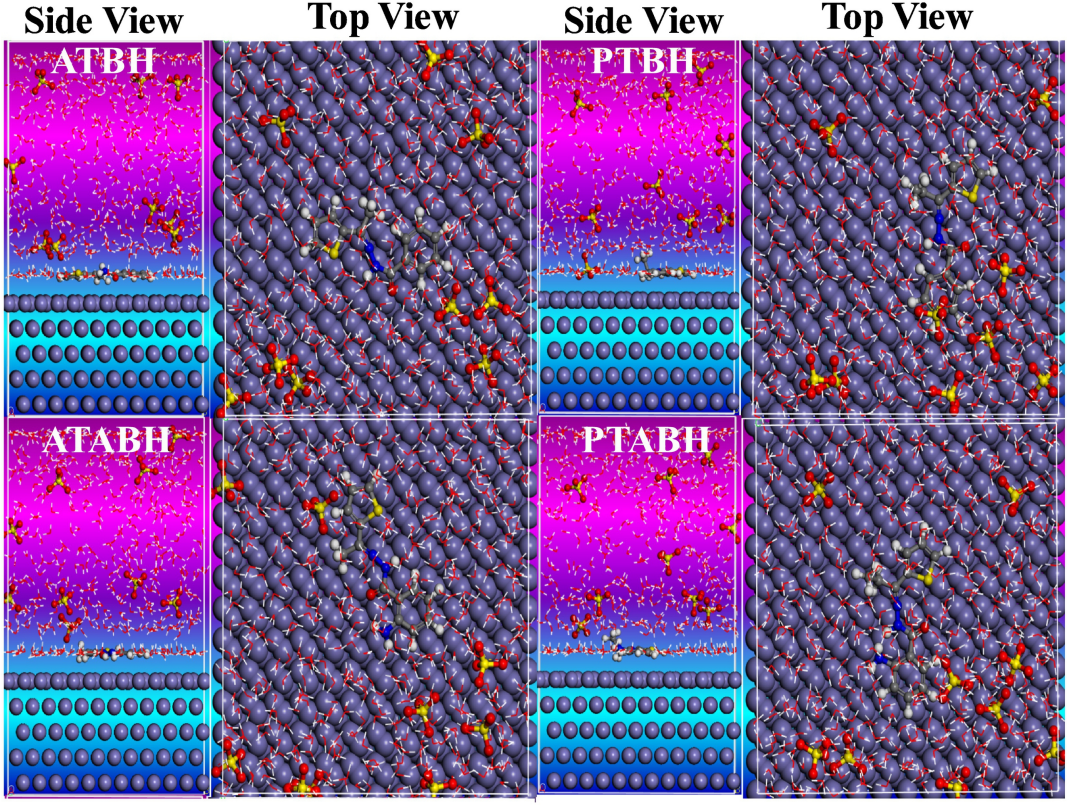

Figure 12